ANALYSIS OF OSCILLATING FLOW COOLED SMA ACTUATOR

A Thesis

by

RAJAGOPAL PACHALLA SESHADRI

Submitted to the Office of Graduate Studies of
Texas A&M University
in partial fulfillment of the requirements for the degree of

MASTER OF SCIENCE

August 2004

Major Subject: Aerospace Engineering

ANALYSIS OF OSCILLATING FLOW COOLED SMA ACTUATOR

A Thesis

by

RAJAGOPAL PACHALLA SESHADRI

Submitted to Texas A&M University
in partial fulfillment of the requirements
for the degree of

MASTER OF SCIENCE

Approved as to style and content by:

Sharath S. Girimaji (Co-Chair of Committee)	Ali Beskok (Member)
Dimitris C. Lagoudas (Co-Chair of Committee)	Walter E. Haisler (Interim Head of Department)

August 2004

Major Subject: Aerospace Engineering

ABSTRACT

Analysis of Oscillating Flow Cooled SMA Actuator. (August 2004)
Rajagopal Pachalla Seshadri, B.Tech., Indian Institute of Technology, Madras, India
Co-Chairs of Advisory Committee: Dr. Sharath S. Girimaji
Dr. Dimitris C. Lagoudas

Shape Memory Alloys (SMA) are a group of metallic alloys that have the ability to return to some previously defined shape or size when subjected to an appropriate thermal cycling procedure. In recent years there has been a lot of research on the development of small, light and, yet, powerful actuators for use in areas like robotics, prosthetics, biomimetics, shape control and grippers. Many of the miniaturized conventional actuators do not have sufficient power output to be useful and SMAs can be used advantageously here.

The widespread use of SMAs in actuators is limited by their low bandwidth. Use of SMAs in two-way actuators requires that they undergo thermal cycling (heating and cooling). While SMAs can be heated quickly by resistive heating, conventional convection cooling mechanisms are much slower as the exothermic austenitic to martensitic phase transformation is accompanied by the release of significant amount of latent heat.

While a number of cooling mechanisms have been studied in SMA actuator literature, most of the cooling mechanisms involve unidirectional forced convection. This may not be the most effective method. Oscillating flow in a channel can sometimes enhance heat transfer over a unidirectional flow. One possible explanation for this heat transfer enhancement is that the oscillatory flow creates a very thin Stokes viscous boundary-layer and hence a large time-dependent transverse temperature gradient at the heated wall. Therefore heat transfer takes place at a large temperature difference, thereby enhancing the heat transfer.

In this work, the heat transfer from an SMA actuator under an oscillating channel is investigated and is compared to steady, unidirectional flow heat transfer.

Oscillating flow is simulated using a finite volume based method. The resulting velocity field is made use of in solving the heat transfer problem using a finite difference scheme. A parametric study is undertaken to identify the optimal flow conditions required to produce the maximum output for a given geometry of the SMA actuator. The latent heat of transformation of the SMA is accounted for by means of a temperature dependent specific heat.

To my parents, my brother and my sister for their patience and sacrifces, and to SK7

ACKNOWLEDGEMENTS

I would like to express my gratitude and appreciation to my advisors, Dr. Dimitris Lagoudas and Dr. Sharath Girimaji, for their guidance and support. Dr. Girimaji showed a lot of patience with me and gave me a second chance and for this I will always be grateful. I would also like to thank Dr. Ali Beskok for the numerous useful discussions we had and for his continued guidance of my research.

I also thank the administrative staff of the Department of Aerospace Engineering for their timely help and their cooperation with paperwork and other administrative matters. I would like to thank Ms. Karen Knabe, Ms. Donna Hollick and Ms. Pam McConal in particular for all their efforts.

I had a number of useful discussions with various graduate students and would like to thank Pavlin Entchev, Mughees Khan and Hyoung Yoll-Jun.

I am also thankful to my friends Sathya, Ashwin, Amarnath, Murali and Sriram for all their help and for being there during tough times.

My parents have sacrificed a lot to get me here and for that I will be eternally grateful. I am also thankful to my brother and my sister for their love and affection and support.

TABLE OF CONTENTS

LIST OF FIGURES

Page

Page

NOMENCLATURE

$\Delta x, A_o$ dimensional and non-dimensional tidal displacement

b thickness of SMA strip

B $\dfrac{\rho_w C_{Pw} b}{\rho_f C_{Pf} R}$

Bi biot number

C_p constant pressure specific heat

h heat transfer coefficient

k thermal conductivity

L hannel length

M Martensite temperature

Nu Nusselt number

p pressure

Pr Prandtl number

R channel height

Re Reynolds number

Re_w oscillatory Reynolds number

t, τ dimensional and dimensionless time

T temperature

u dimensional axial velocity

u_m dimensional inlet velocity magnitude

x, X dimensional and non-dimensional axial distance

y, Y dimensional and non-dimensional transverse distance

Greek symbols

α Womersley number

α_f thermal diffusivity ($k/(\rho C_p)$)

δ Stokes boundary layer thickness

ν kinematic viscosity of fluid

ρ density

θ non-dimensional temperature

ω flow frequency

Ω actuation frequency

Subscripts

b bulk property

E entrance

f fluid

r reference

w wall/ SMA

Superscript

0 initial value

f forward transformation

fi finish temperature

r reverse transformation

st start temperature

CHAPTER I

INTRODUCTION AND LITERATURE REVIEW

In recent years there has been a lot of research on the development of small, light and, yet, powerful actuators for use in areas like robotics, prosthetics, biomimetics, shape control and grippers. Many of the miniaturized conventional actuators do not have sufficient power output to be useful and SMAs can be used advantageously here. SMAs came into prominence after the discovery of Ni-Ti SMAs by Buehler and Wiley [1] in the 1960's. Shape Memory Alloys (SMA) are a group of metallic alloys that have the ability to return to some previously defined shape or size when subjected to an appropriate thermal cycling procedure [2]. SMAs can transform from the high temperature parent phase (austenite) to the low temperature phase (martensite) upon cooling, and upon heating above the austenitic finish temperature the parent phase is recovered with very little hysteresis. Due to this transformation, two types of behavior can occur in SMAs, namely pseudoelastic effect and shape memory effect (SME) [3], of which the SME is used in actuators. SMAs also have high damping capacity and can be used as structural dampers. Lagoudas et al. [4] studied the vibration isolation characteristics of a SMA material and proposed a simplified model for the pseudo elastic response.

The widespread use of SMAs in actuators is limited by their low bandwidth. Use of SMAs in two-way actuators requires that they undergo thermal cycling (heating and cooling). While SMAs can be heated quickly by resistive heating, conventional convection cooling mechanisms are much slower [5] as the exothermic austenitic to martensitic phase transformation is accompanied by the release of significant amount of latent heat.

This thesis follows the style and format of the International Journal of Heat and Mass Transfer.

The cooling time can be reduced by a low temperature ambient surrounding the SMA actuator, as well as by increasing the convection coefficient. This increases the heat transfer rate but at the same time it also increases the power required to heat the SMA to actuation temperature. A balance has to be achieved between the efficiency of the cooling and the power supplied to SMA based on the total energy cost. Stalmans [6] and Rediniotis et al. [7] proposed use of rectangular strips instead of round wires, forced convection cooling by a moving liquid and miniaturization of the actuator to increase the frequency response of SMA actuators.

Current work on SMA actuators

SMAs can be trained to undergo two-way transformation at large transformation strains up to 3%. SMAs have high power to weight ratio and this makes them a very attractive material for use in high force actuators. The ability to be fabricated into almost any shape is also a big advantage of SMAs. A single electrically actuated SMA wire can sometimes be used as an actuator without the need for any additional parts.

Rediniotis et al. [7] introduced a new idea for a fuel powered compact SMA actuator cooled by forced convection. They simulated the heat transfer from a strip of SMA under unidirectional forced convection and compared their results with experiments. The commercial CFD software package FLUENT was used for the simulation with the specific heat of the SMA being modeled in a piecewise manner to account for the latent heat of transformation. Their simulation showed a frequency of 0.5 Hz was attainable for a SMA strip of thickness 1mm. Brinson et al. [8] formulated a coupled thermomechanical problem of a resistively heated and convection cooled SMA wire undergoing transformation and deformation. They solved the decoupled thermal problem assuming a convective heat transfer coefficient and predicted the mechanical response based on the temperature of the SMA strip. Ho et al. [9] used a finite difference method to solve for the response of a thin film SMA undergoing resistive heating and forced convection cooling. Their calculation included the assumption of a heat transfer coefficient for the forced convection and that the phase transformation occurs at fixed

temperature. Their simulations showed a peak frequency of 69 Hz for a 4 μm SMA strip actuator. Their calculation also indicated a dependence of the frequency response not only on the transformation temperatures, but also on their ratios.

Lagoudas and Kinra [10] proposed a novel idea for a SMA actuator with cooling based on the Peltier effect. Their design featured a thin layer of SMA sandwiched between a pair of positively and negatively doped semiconductor elements. The SMA forms two junctions, one with each of the semiconductors. When current flows through the junctions, heat is transferred in the direction of the current at the first junction and against the direction of the current at the other junction. Thus the SMA is heated by the semiconductors acting as heat sources. When the direction of current is reversed, the opposite occurs and the SMA is in effect cooled by the semiconductors now acting as heat sinks. Bhattacharyya et al. [11] formulated the heat transfer model for a thermoelectric cooled SMA actuator by assuming that the temperature field was one-dimensional. Their numerical calculation showed the temperature field was uniform in the SMA. Lagoudas and Ding [12] studied the problem of thermal cycling (alternate heating and cooling) in a thin layer SMA actuator using the uniform temperature field result of [11]. They also assumed a one-dimensional temperature field in the semiconductor elements.

Brailkovski et al. [13] predicted the thermomechanical response of a SMA wire actuator based on a new interpolation technique called dual krigging for the mechanical response and coupled it with the thermal model. They developed a simple analytical model based on energy balance to estimate the temporal characteristics of the SMA actuator. A convective heat transfer coefficient was assumed to solve the thermal problem. Lagoudas and Bhattacharyya [14] solved the coupled thermomechanical problem for a thin layer extensional SMA actuator, again using the uniform temperature field result of [11] for the SMA. Their numerical results showed that it was possible to achieve a frequency of about 30 Hz for a thin layer SMA (~ 6μm) at a stress of 145 MPa.

Oscillatory flow heat transfer

Heat transfer in a steady, unidirectional pressure driven flow (Poiseuille's flow) is relatively simple to analyze but it is not always the most effective method of cooling. Previous studies have shown that an oscillating flow in a heated channel can enhance heat transfer over steady unidirectional flow. Heat transfer in oscillating flow is enhanced by heat conduction in high frequency-low amplitude oscillatory flow and by forced convection in low frequency-large amplitude of oscillations. Warburton and Beskok [15] and Sert and Beskok [16] simulated the heat transfer in a micro heat spreader device based on oscillating flow. They conclude that although steady unidirectional forced convection cooling produced lower surface temperatures than the oscillating flow, a suitable combination of flow and device parameters may produce higher heat transfer rates in the reciprocating flow.

Kurzweg [17] found that the axial heat transferred in oscillating flows between a hot and a cold reservoir can be orders of magnitude larger than pure molecular conduction. One possible explanation for this heat transfer enhancement is that the oscillatory flow creates a very thin Stokes viscous boundary-layer and hence a large time-dependent transverse temperature gradient at the heated wall [18]. Therefore a large amount of heat is transferred to the fluid core (bulk) from the wall through the boundary layer. The periodic interaction of axial convection with this transverse heat flow to the fluid core from the boundary layer produces an enhanced net heat transfer from the hot reservoir to the cold reservoir. Richardson [19] showed that the velocity profile for a pulsating flow is steeper nearer the wall than it is in the steady flow, and that the maximum fluid velocity occurs near the walls rather than the center of the channel. Moschandreou and Zamir [20] suggested that the temperature profile must be affected similarly by an oscillating flow thus resulting in an increase in the heat transfer rate. Their explanation of the mechanism of heat transfer enhancement and sometimes degradation in oscillating flows is that the pulsating nature of flow alters the bulk temperature and allows heat transfer to take place at a larger (enhancement) or smaller

(degradation) temperature difference. The heat transfer rate increases with increase in frequency but there is a peak beyond which the heat transfer decreases.

Research objectives and thesis outline

The main objective of this thesis is to formulate the heat transfer problem for a SMA actuator heated by resistive heating and cooled by forced convection and to compute solutions for oscillating flows in a 2-D channel. First, a simplified model for heat transfer from the SMA in a unidirectional laminar flow is introduced. The heat transfer problem for a steady state, unidirectional, incompressible and viscous flow in a 2-D channel where one wall is a SMA strip, is solved by assuming a parabolic velocity profile. The coupled energy equations for the fluid and SMA strip are solved together using a finite difference method [21]. The heat transfer analysis in the oscillating flow is then performed. A finite volume code based on the SIMPLER algorithm [22] has been developed to simulate an oscillating laminar flow in a 2-D channel. After the velocity field is calculated for each time step, the heat transfer problem is solved.

The phase transformation of the SMA is accompanied by release or absorption of latent heat of phase change. This latent heat is accounted for by means of a temperature dependent heat capacity of the SMA [7] and [11].

The results from the steady, unidirectional flow and the oscillating flow are compared. A compact SMA actuator based on the oscillating flow is designed based on a parametric study, to determine the geometry of the actuator (channel height and SMA strip thickness) and the flow conditions parametrized by frequency of actuation, frequency of oscillation of the flow, temperature of fluid at inlet, amplitude of the tidal displacement.

The outline of the thesis is as follows. The concept of the device is explained in Chapter II. The model for heat transfer from a strip of SMA under steady unidirectional forced convection is presented. General characteristics of oscillating flows are also introduced and equations of energy for the fluid and the SMA are written in the non-dimensional form. The full finite volume simulation of oscillating flow in a 2-D channel

is explained in Chapter III and Chapter IV is devoted to the results of the simulations. Chapter V contains discussion of the results and future work. The appendix contains description of how the latent heat of transformation of the SMA is taken into account for the heat transfer analysis.

CHAPTER II

MODEL FOR HEAT TRANSFER

Unidirectional flow forced convection

One of the simplest ways of cooling a hot body is by forced convection. Sucec [21] and [24] presents a finite difference method to solve for transient heat transfer in channel with spatially sinusoidal and time varying heat generation inside the wall. The objective here is to study the conjugate heat transfer problem in a 2-D channel with one of the walls being an SMA strip. A fully developed flow (parabolic velocity profile) is assumed. Fluid enters the channel at a constant temperature of T_E. The formulation outlined in [24] is used in this study.

Since the SMA strip is at the center of the channel (Figure II.1), only the symmetrical half of the channel and SMA strip system (Figure II.2) is studied.

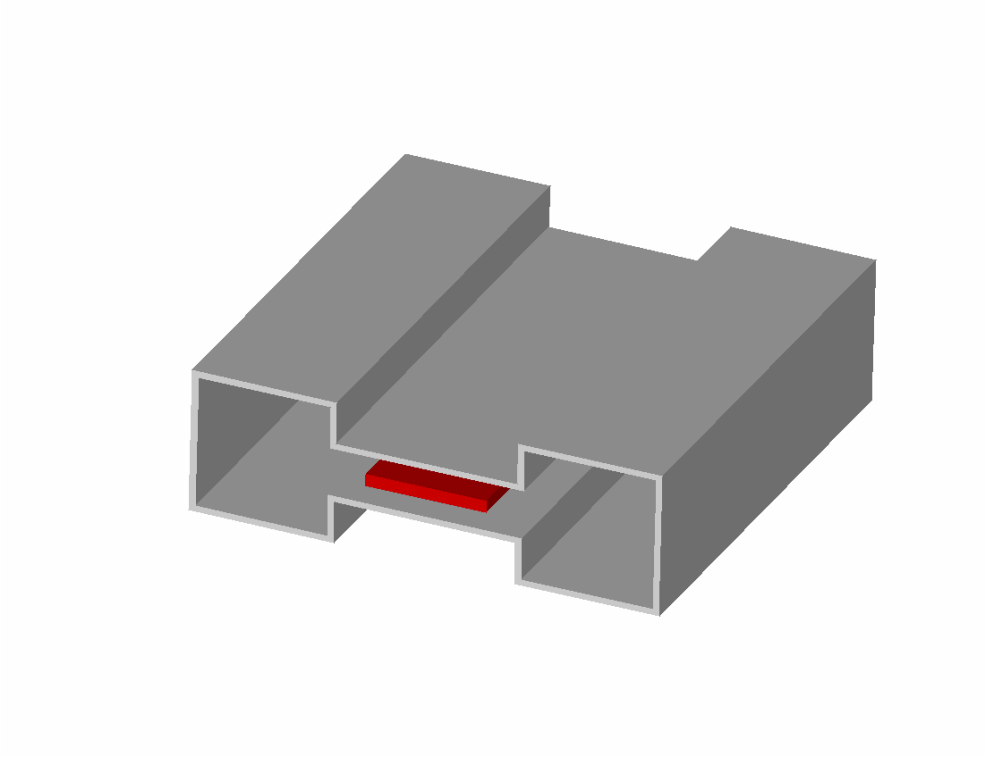

Figure II.1. Schematic of SMA actuator

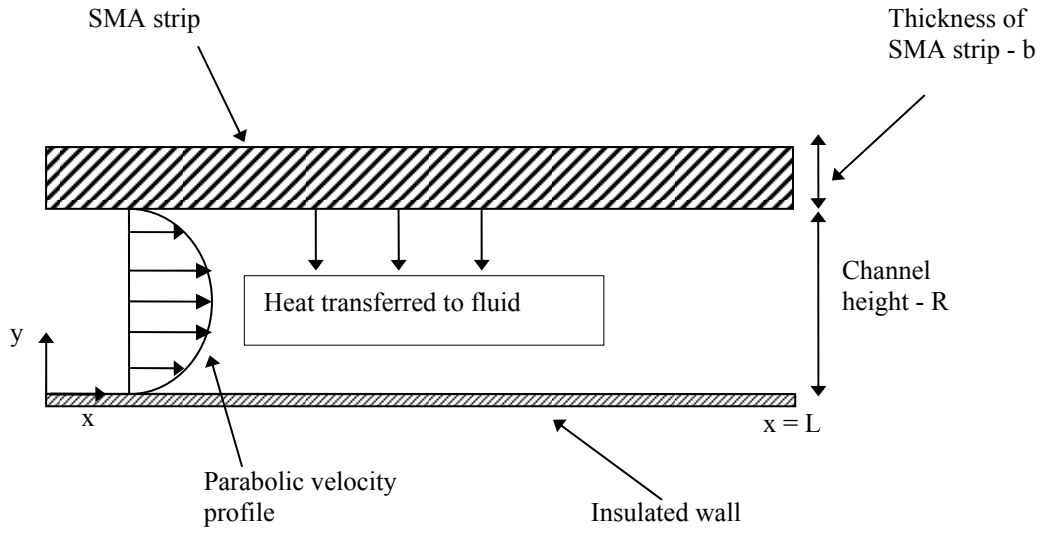

Figure II.2. Schematic of heat transfer in channel (symmetric half shown)

Assuming the heat capacity and the thermal conductivity of the fluid to be constant, the energy equation for the fluid is [24]

$$\rho_f C_{pf} \frac{\partial T_f}{\partial t} + \rho_f C_{pf} u(y) \frac{\partial T_f}{\partial x} = k_f \left(\frac{\partial^2 T_f}{\partial x^2} + \frac{\partial^2 T_f}{\partial y^2} \right) \quad \text{(II.1)}$$

The initial condition for the fluid and the SMA strip is given by

$$T = T_E,\ t = 0,\ 0 \le x \le L,\ 0 \le y \le R \quad \text{(II.2)}$$

And the temperature of the fluid at the inlet is

$$T = T_E,\ x = 0,\ t > 0,\ 0 < y < R \quad \text{(II.3)}$$

The lower wall of the channel is assumed to be insulated. This boundary condition is written as

$$\frac{\partial T}{\partial y} = 0,\ y = 0,\ t > 0,\ 0 \le x \le L \quad \text{(II.4)}$$

The boundary condition at the exit of the channel is

$$\frac{\partial T}{\partial x} = 0 \text{ , } t > 0,\ 0 < y < R,\ x = L \qquad \text{(II.5)}$$

And $u(y)/U_{max} = 4((y/R) - (y/R)^2)$ where U_{max} is the maximum velocity (occurs at the centre of the channel). U_{max} is selected to set the Reynolds number appropriately.

The energy balance for the SMA strip is written as

$$\rho_w C_{pw} b \frac{\partial T_w}{\partial t} + k_w \frac{\partial T_w}{\partial y} = f q_g b + k_w \frac{\partial^2 T_w}{\partial x^2} \text{ , } t > 0,\ x > 0,\ y = R \qquad \text{(II.6)}$$

The temperature and heat flux at the interface of the fluid and the SMA strip are continuous, so we have

$$T_w \big|_{y=R} = T_f \big|_{y=R}$$
$$k_w \left.\frac{\partial T_w}{\partial x}\right|_{y=R} = -k_f \left.\frac{\partial T_f}{\partial x}\right|_{y=R} \qquad \text{(II.7)}$$

Using II.6, the energy balance for the SMA strip can be rewritten as

$$\rho_w C_{pw} b \frac{\partial T_f}{\partial t} - k_f \frac{\partial T_f}{\partial y} = f q_g b + k_w \frac{\partial^2 T_f}{\partial x^2} \text{ , } t > 0,\ x > 0,\ y = R \qquad \text{(II.8)}$$

Where the non-dimensional heat supplied is $f = \frac{q_{sup}}{q_g}$. The quantity q_{sup} represents the heat supplied to the SMA strip to transform it into austenite, while q_g is used to non-dimensionalize q_{sup} and both have units W/m^3. Here the subscript f refers to the fluid and w to the wall, C_{pf} and C_{pw} are the specific heats of the fluid and SMA respectively, T_E is the entry fluid temperature, b is the SMA strip thickness and R is the channel height. The specific heat of the SMA has to be modified as a function of temperature to take into account the latent heat of phase transformation (APPENDIX A).

The equations of energy balance for the fluid and the SMA strip are non-dimensionalized and solved using a finite-difference method [21] and [24]. The source term in the energy equation (6) for the SMA, fq_gb, represents resistive heating. To

simulate the heat transfer for an actuator frequency of $\Omega = 2\pi/\tau$, where τ is the period of one actuation cycle, f is set to a constant non-zero value for half the cycle during resistive heating. It is set to zero during the other half of the cycle to simulate cooling by forced convection.

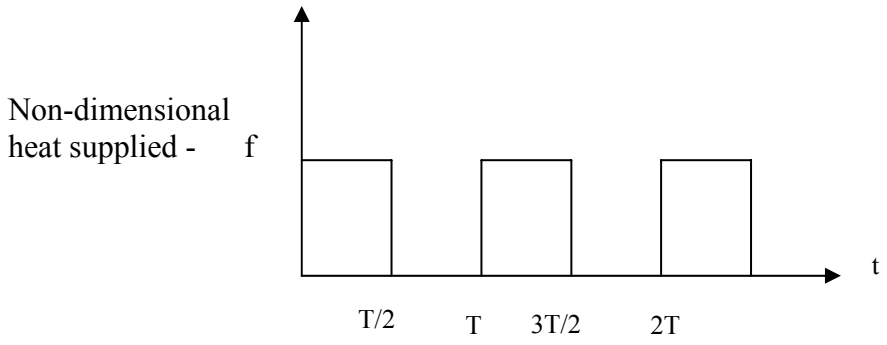

Figure II.3. Heat supplied for actuating frequency $\Omega = 2\pi/T$, as a function of time

The strain output is directly proportional to the volume fraction of SMA that is transformed to austenite upon heating and then to martensite on cooling. A parametric study is done to identify the flow conditions and device geometry that would maximize this volume fraction of the SMA, which is in both the austenite and martensite phase, for various frequencies of actuation.

The energy equation of the fluid (II.1) can be written in non-dimensional form as (APPENDIX B)

$$\frac{\partial \theta_f}{\partial \tau} + 4(Y - Y^2)\frac{\partial \theta_f}{\partial X} = \frac{\partial^2 \theta_f}{\partial Y^2} \quad , \tau > 0,\ X > 0,\ 0 < Y < 1 \qquad \text{(II.9)}$$

where θ_f is the non-dimensional fluid temperature. The energy balance equation for the SMA (II.6) in non-dimensional form (APPENDIX B) is

$$B\frac{\partial \theta_w}{\partial \tau} - \left(\frac{\partial \theta_w}{\partial Y}\right) = f \quad , \tau > 0,\ X > 0,\ Y = 1 \qquad \text{(II.10)}$$

The initial condition (II.2) is given in non-dimensional form by

$$\theta = 0, \tau = 0 : X > 0, 0 \le Y \le 1 \qquad \text{(II.11)}$$

and the temperature of the fluid at the inlet (II.3) is set as

$$\theta = 0, X = 0 : \tau > 0, \ 0 < Y < 1 \qquad \text{(II.12)}$$

The bottom wall of the channel is insulated (II.4). In terms of non-dimensional variables this is written as

$$\frac{\partial \theta}{\partial \tau} = 0 \text{ , } Y = 0, \tau > 0, X > 0 \qquad \text{(II.13)}$$

The boundary condition at the exit of the channel (II.5) is given by

$$\frac{\partial \theta}{\partial X} = 0 \text{ , } \tau > 0, 0 < Y < 1, X = L/R \qquad \text{(II.14)}$$

where $\theta = \dfrac{k_f (T - T_E)}{qbR}, \tau = \alpha_f t / R^2, Y = y / R, X = \alpha_f x / (R^2 U_{\max}), B = \dfrac{\rho_w C_{Pw} b}{\rho_f C_{Pf} R}$.

The symbol τ denotes the non-dimensional time and B is a non-dimensional parameter that is the ratio of heat capacities of the SMA and the fluid. f is a non-dimensional measure of heat supplied to the wall and can be a function of both time and space. In the above equations, subscript f refers to the fluid and subscript w refers to the wall/SMA.

The axial conduction of heat in both the fluid and the wall is neglected. This is justified if the ratio of thermal conductivities of wall to fluid is high (~1000) [24]. In the present study, the ratio of the thermal conductivities of the SMA and the fluid is 30. So we are justified in neglecting axial conduction in the SMA strip.

Also, if we include the axial conduction in the SMA strip, the equation of energy balance becomes

$$B \frac{\partial \theta}{\partial \tau} - \left(\frac{\partial \theta}{\partial Y}\right) = f + \left(\frac{k_w}{k_f}\right)\left(\frac{b}{R}\right) \frac{1}{\mathrm{Re}^2 \, \mathrm{Pr}^2} \frac{\partial^2 \theta}{\partial X^2} \qquad \text{(II.15)}$$

We can see that the axial conduction term is inversely proportional to the square of the Reynolds number and the Prandtl number. Therefore the axial conduction term is neglected. So we have 2 reasons to justify neglecting axial conduction within the SMA strip.

It is also assumed that the temperature gradient along the thickness of the SMA strip is negligible. The magnitude of temperature gradient in the SMA strip is determined by the Biot number (Bi), which is defined as

$$Bi = \frac{hb}{k} \tag{II.16}$$

Where h is the equivalent heat transfer coefficient, b is the thickness and k is the thermal conductivity. Bi can be interpreted as the ratio of internal resistance to heat transfer in the SMA and the external resistance to heat transfer to the fluid. If Bi is much less than 1.0, then the temperature gradients are small and the assumption made here is valid. In this work b is of the order of 1mm (10^{-3} m), k is 30 W/m/K and h is O(1). Biot number is small compared to one and hence the assumption made here is reasonable and the cooling is limited only by convection.

The latent heat released during the forward transformation (exothermic) and absorbed during the reverse transformation (endothermic) is represented through a temperature dependent specific heat for now (APPENDIX A).

Results

The heat transfer problem defined by Equations II.9–II.14 is solved numerically using a finite difference scheme detailed in Sucec ([21] and [24]). The thickness of the SMA is taken to be 0.25 mm, while the length of the channel is 2 cm. The height of the channel is varied between 0.2 and 1 mm. The temperature of fluid at inlet (T_E) is given three values, namely 45°, 50° and 55° C. The Reynolds number is varied by varying the channel height and U_{max}.

The SMA undergoes transformation over a temperature range and therefore any point on the SMA strip with a temperature within the range exists as both austenite and martensite simultaneously. The force output of the type of SMA actuator considered in

this work is directly proportional to the volume of SMA that is completely transformed to austenite during reverse transformation and to martensite during forward transformation. In other words, this volume exists only as austenite after heating and only as martensite after cooling. This volume percentage is plotted in Figure II.4-II.7 as a function of the channel height for various Reynolds numbers.

When the heat supplied in not sufficient (Figure II.4), the volume undergoing complete transformation is very small. As the heat supplied to the SMA increases, we see that the volume undergoing complete transformation increases dramatically (Figure II.5-II.6). There is a decrease in the volume in Figure II.7 because the initial temperature in high and there isn't enough cooling for transformation to martensite.

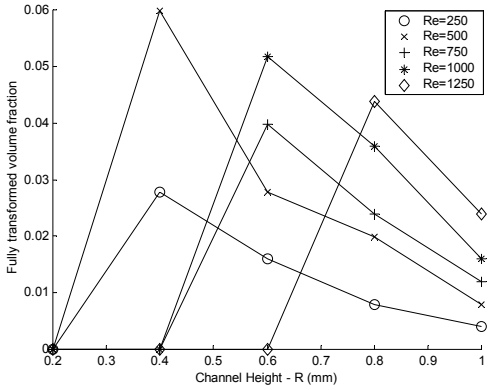

Figure II.4 $T_E = 50°$ C, f = 2

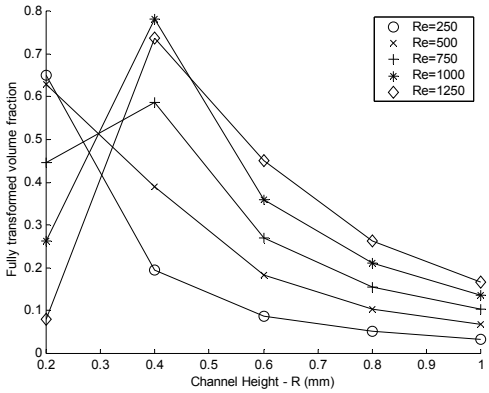

Figure II.5 $T_E = 50°$ C, f = 4

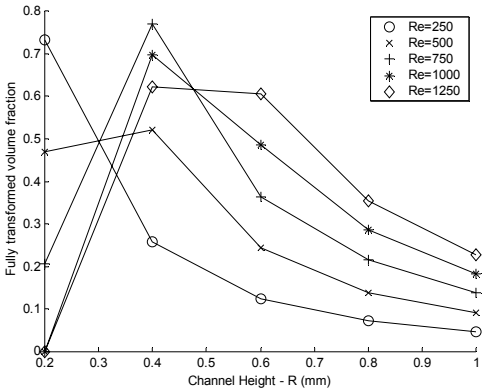

Figure II.6 $T_E = 45°$ C, f = 4

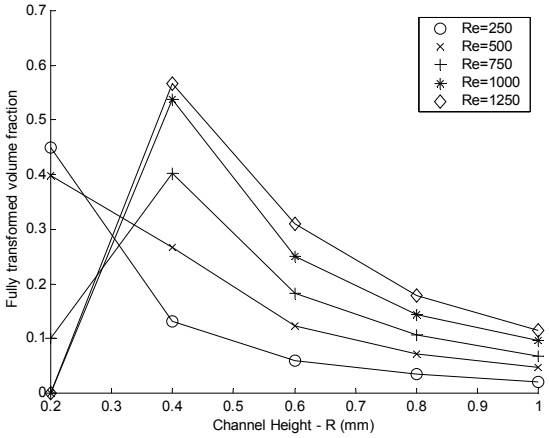

Figure II.7 $T_E = 55°$ C, f = 4

Concept of the oscillating flow SMA actuator

The SMA actuator is resistively heated and cooled by oscillatory flow forced convection. The actuator provides linear motion and heat flow takes place in a perpendicular direction. This allows for modular design and multiple SMA elements in the channel. The cooling system under investigation is based on the concept of a micro heat spreader system introduced by Warburton and Beskok [15] and Sert and Beskok [16]. It consists of two reservoirs connected by a micro-channel (Figure II.1 and Figure II.8). The fluid can be pumped by piezoelectrically actuated reservoir wall membranes or by pistons in the two reservoirs. Electrostatic actuation of micro-membranes has been

successfully achieved and documented in [23]. Continuous actuation of the membranes or pistons ensures a continuous flow of fluid from one reservoir to the other.

This design of the actuator provides for two forced convection cooling passes per membrane or piston cycle and increases the cooling effectiveness. As the channel height is reduced, heat transferred from the SMA to the fluid increases, but it decreases if the height is reduced beyond a particular value as the fluid is heated very quickly and heat transfer has to take place at a smaller temperature difference. The fluid is pumped from one reservoir into the channel and is heated by the SMA. The fluid is then pushed into the receiving reservoir and recirculates with the cooler fluid.

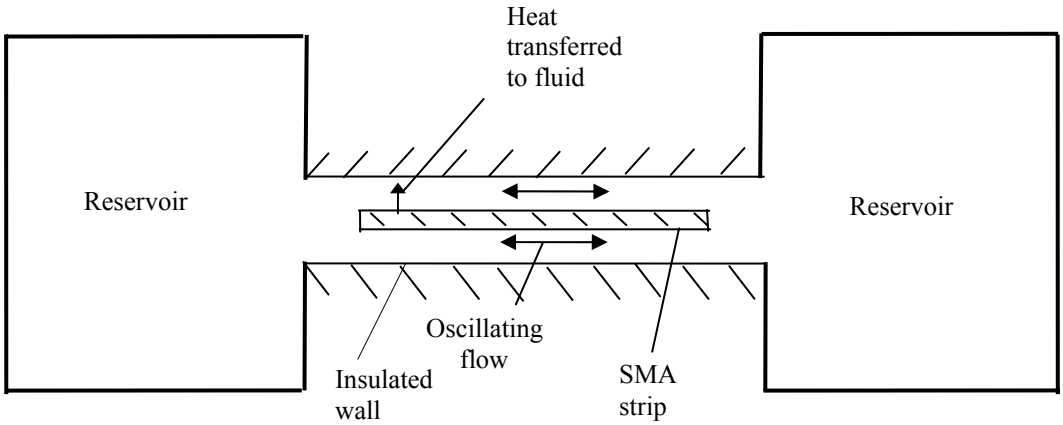

Figure II.8. Side view of SMA actuator

Important parameters in oscillating flow

The steady unidirectional flow forced convection discussed in the previous section is not the most effective way for cooling. Kurzweg [17] studied axial dispersion of contaminants in steady laminar and oscillatory laminar flows and found that there was an enhancement in transport of the contaminants in the oscillatory flow over the steady laminar flow. He suggested that a similar dispersion process should occur during heat transfer because of the similarity of the governing equations. Kurzweg also found that

the axial heat transferred in oscillating flows between a hot and a cold reservoir can be orders of magnitude larger than pure molecular conduction.

One possible explanation for this heat transfer enhancement is that the oscillatory flow creates a very thin Stokes viscous boundary layer and hence a large time-dependent transverse temperature gradient at the heated walls [25]. Therefore a large amount of heat is transferred to the fluid core (bulk) from the boundary layer and in turn from the wall. The periodic interaction of axial convection with this transverse heat flow to the fluid core from the boundary layer produces an enhanced net heat transfer from the hot reservoir to the cold reservoir.

Consider an oscillating flow with a frequency ω. Consider the time and cross-averaged displacement of particles defined by

$$\Delta x = \frac{1}{R}\int_{-\pi/\omega}^{\pi/\omega} dt \int_{-R/2}^{R/2} u(y,t)dy \qquad \text{(II.17)}$$

Δx is referred to as the tidal displacement.

The half-cycle mean fluid velocity is given by

$$u_m = \frac{1}{R}\int_{-\pi/\omega}^{\pi/\omega} dy \frac{\omega}{\pi} \int_{-R/2}^{R/2} u(y,t)dy \qquad \text{(II.18)}$$

This mean fluid velocity, u_m, is used as the characteristic velocity while non-dimensionalising the governing equations. We can also define an oscillatory Reynolds number as $\mathbf{Re}_w = \frac{\omega R^2}{\nu}$.

The Wormersley number is defined as

$$\alpha = R\sqrt{\frac{\omega}{\nu}} = \sqrt{\mathbf{Re}_w} \qquad \text{(II.19)}$$

The tidal displacement, Δx, is closely related to the amplitude of the pressure gradient. Larger the amplitude of the pressure gradient, larger the Δx (axial excursion of fluid particles during a half-cycle) and more fluid is pumped during a half-cycle. A non-dimensional tidal displacment can be defined as $A_0 = \Delta x/R$.

Zhao and Cheng [27] found that Re_w, Pr (Prandtl number), A_0 and L/R were similarity parameters for heat transfer in an oscillating flow. A larger tidal displacement means that fluid that is heated by the heat transfer from the wall travels very far and may even go into the exit reservoir. This means that during the second half of the cycle fluid that is cooler is pumped into the channel and a greater heat transfer takes place than if the tidal displacement were smaller. Therefore Re_w and A_0 are the most important parameters influencing the heat transfer to an oscillating flow. Some experimental studies show that heat transfer is increased when the oscillation frequency (and hence Re_w) is increased.

The results of various studies done on heat transfer in pulsating and oscillating flows make it a very interesting option to use in the design of compact SMA actuators.

Heat transfer in laminar oscillating flow

Ozawa et al. [28] numerically solved the problem of heat transfer in an oscillating channel flow by assuming an analytical solution for the fully developed velocity profile. They compared the cycle-averaged (time-averaged) Nusselt number with experimental results and found a very good match for laminar flows.

For an oscillating flow in a 2-D channel, the u-momentum equation with the convection terms neglected is given by

$$\frac{\partial u}{\partial t} = -\frac{1}{\rho}\frac{\partial p}{\partial x} + \nu\frac{\partial^2 u}{\partial y^2} \tag{II.20}$$

Where $\frac{1}{\rho}\frac{\partial p}{\partial x} = -K\cos(\omega t)$ and ωt is the phase angle.

The analytical solution of (20) can be written as [29]

$$u(y,t) = a(y)\cos(\omega t) + b(y)\sin(\omega t) \tag{II.21}$$

where

$$a(y) = K\left[\frac{\cosh\alpha y\cos\alpha(R-y) + \cos\alpha y\cosh\alpha(R-y)}{\cosh\alpha R + \cos\alpha R}\right] \tag{II.22}$$

and

$$b(y) = K\left[\frac{\sinh \alpha y \sin \alpha(R-y) + \sin \alpha y \sinh \alpha(R-y)}{\cosh \alpha R + \cos \alpha R}\right] \qquad \text{(II.23)}$$

In the above, ω is the frequency of flow oscillation (or frequency of the oscillating pressure gradient) and R is the channel height.

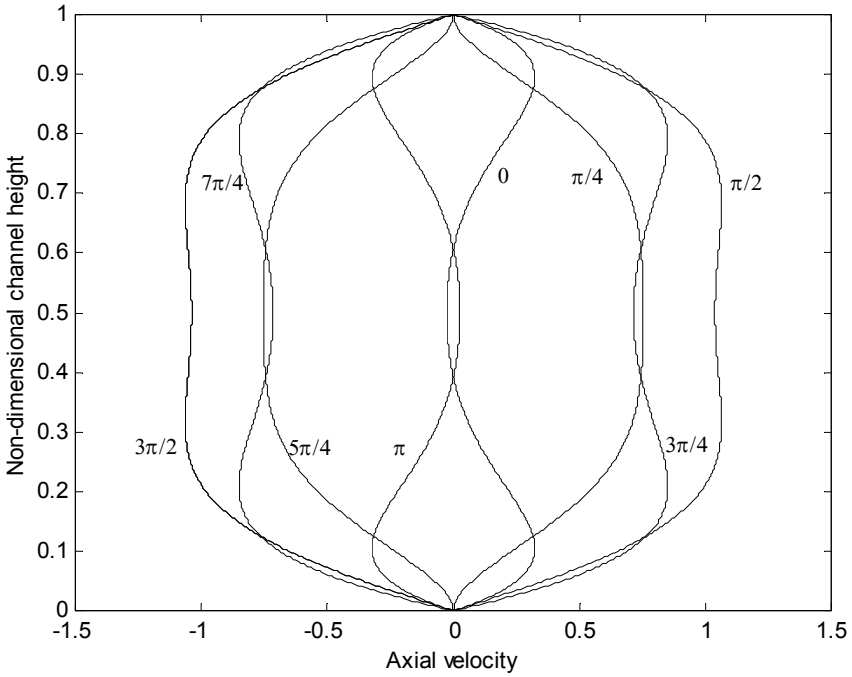

Figure II.9. Theoretical velocity profile as a function of channel

The problem of oscillating flow is solved computationally using a finite-volume code called SIMPLE [22]. The velocity profiles over one period of oscillation is shown below for two values of ω (4 Hz and 10 Hz). At low frequency the oscillating flow has a noticeable shape in the bulk apart from the Stokes boundary layer of thickness $\delta = \sqrt{2\upsilon/\omega}$. But at very low frequencies the profile (Figure II.9) is similar to the commonly observed parabolic profile of unidirectional flow. At high frequencies, the Stokes boundary layer is quite thin and the bulk flow is almost a plug flow (Figure II.10).

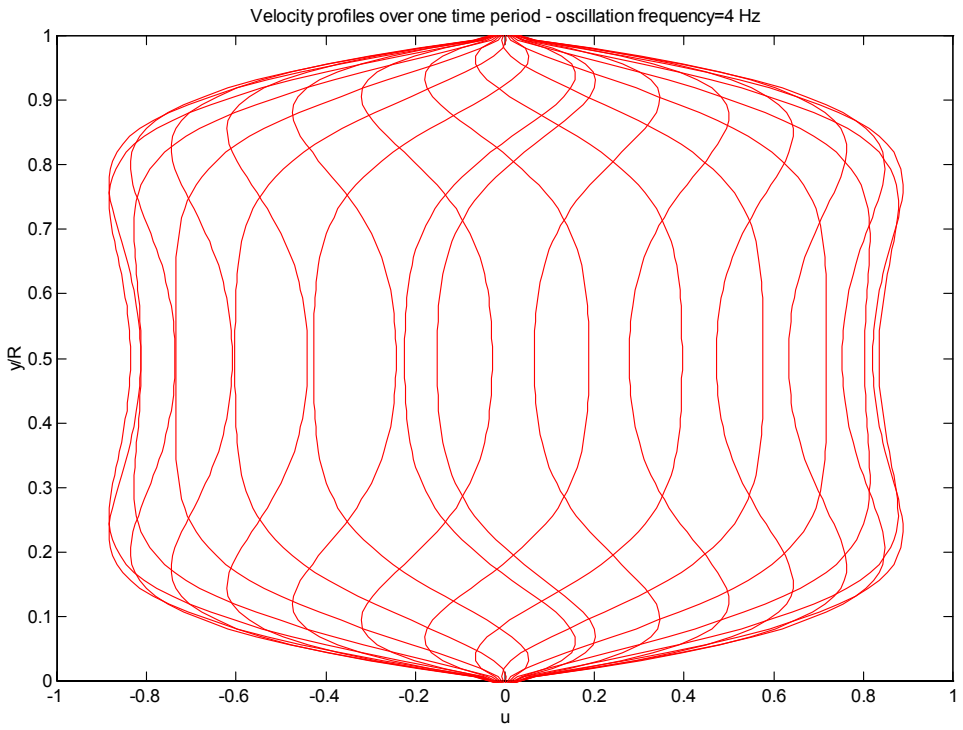

Figure II.10. Simulated velocity profile as a function of channel height for ω = 4 Hz

Figure II.11 shows the effect of increasing oscillation frequency. The bulk of the flow is very flat, showing the plug nature of the bulk flow.

The heat transferred to the fluid from the SMA will not be enhanced much by a high frequency if the molecular conduction of the fluid is small. On the other hand, if the frequency of oscillation is small but the molecular conduction of the fluid is large then again the system is not efficient.

The heat transfer problem for the oscillating flow is solved as before for the unidirectional flow. Here velocity is time varying instead of a simple parabolic profile. Also, the boundary conditions are now time periodic and change after every half cycle (Figure II.12).

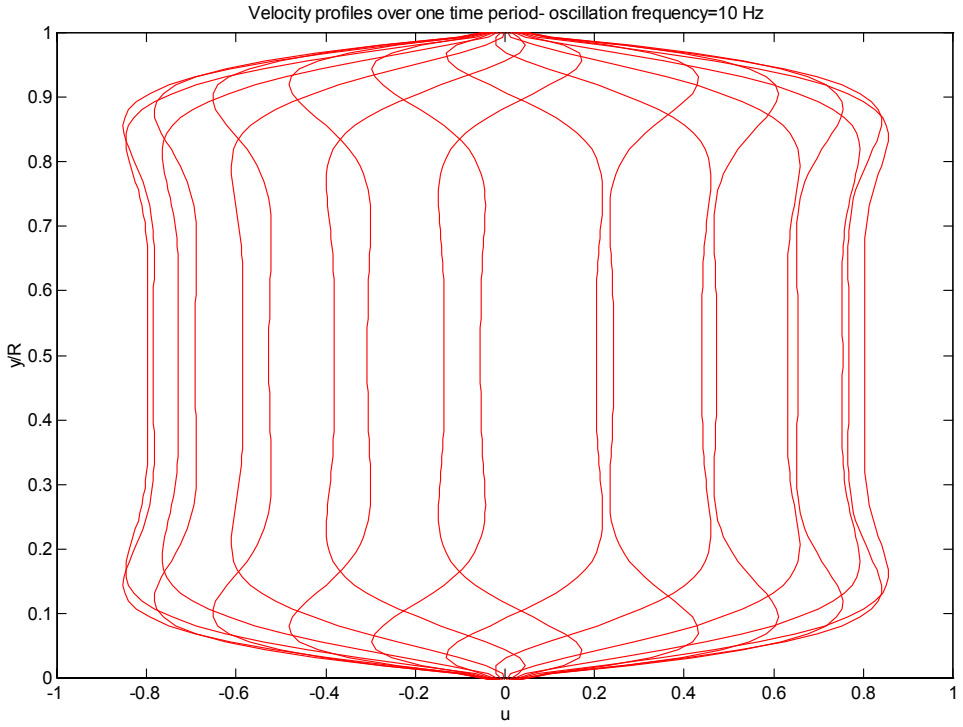

Figure II.11. Simulated velocity profile as a function of channel height for ω = 10 Hz

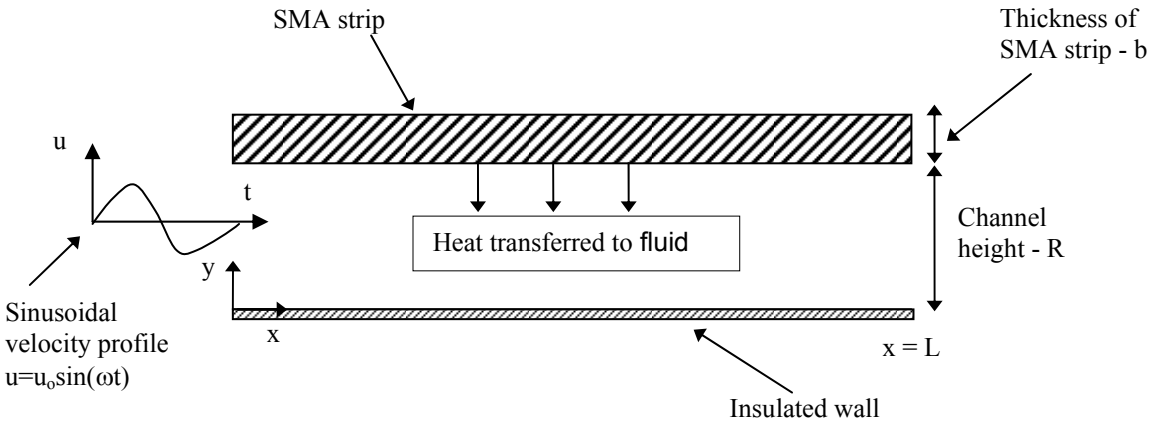

Figure II.12. Schematic of oscillating flow heat transfer in a 2-D channel

Non-dimensionalising Equation (2) gives the following energy equation (APPENDIX B) for the fluid

$$\frac{\partial \theta_f}{\partial \tau} + \frac{A_0}{\pi}\left[U\frac{\partial \theta_f}{\partial X} + V\frac{\partial \theta_f}{\partial Y}\right] = \frac{1}{\mathrm{Re}_w \,\mathrm{Pr}}\left[\frac{\partial^2 \theta_f}{\partial X^2} + \frac{\partial^2 \theta_f}{\partial Y^2}\right], \quad \tau>0,\ X>0,\ 0 < Y < 1 \qquad \text{(II.24)}$$

The non-dimensional form of the energy equation for the SMA strip (Equation (6)) is given by

$$B\frac{\partial \theta_w}{\partial \tau} - \left(\frac{\partial \theta_w}{\partial Y}\right) = f + \left(\frac{k_w}{k_f}\right)\left(\frac{b}{R}\right)\frac{\partial^2 \theta_w}{\partial X^2} \quad ,\ \tau > 0,\ X > 0,\ Y = 1 \qquad \text{(II.25)}$$

The initial condition for the fluid and the SMA strip is

$$\theta = 0,\ \tau = 0,\ X > 0,\ 0 \le Y \le 1 \qquad \text{(II.26)}$$

The boundary condition at the wall (Y = 0) is given by

$$\frac{\partial \theta}{\partial y} = 0\ ,\ \tau > 0,\ X > 0,\ Y = 0 \qquad \text{(II.27)}$$

The temperature of fluid at the inlet is

$$\theta = 0,\ X = 0,\ 0<\tau<\pi,\ 0 < Y < 1 \qquad \text{(II.28)}$$

And the boundary condition at the exit is

$$\frac{\partial \theta}{\partial X} = 0\ ,\ X = L/R,\ 0<\tau<\pi,\ 0 < Y < 1 \qquad \text{(II.29)}$$

Here

$$X = x/R, Y = y/R, U = u/u_{\max}, V = v/u_{\max}, \tau = \omega t, \theta = \frac{T - T_E}{T_r - T_E}, B = \frac{\rho_w C_{Pw} b}{\rho_f C_{Pf} R} * \mathrm{Re}_w \,\mathrm{Pr}$$

The heat supplied to the SMA is now defined in terms of the inlet temperature T_E and the reference temperature, T_r. The dimensional value of the heat supplied is $q_g = f * k_f * (T_r - T_E)/R$ and f is the non-dimensional value of the heat supplied.

After a half cycle ($\omega t = \pi$), the flow direction is reversed. The boundary conditions (28) and (29) are reversed with the fluid entering the channel from X = L/R and exiting at X = 0. ω is the frequency of flow oscillation, τ is the non-dimensional time, θ is the non-dimensional temperature and Pr is the Prandtl number of the fluid. The heat supplied to the SMA is at the frequency of actuation (Ω) required (Figure II.3).

The heat transfer problem defined by Equations II.24-II.29 is solved using the method of Sucec[24], with the velocity profile of Equations II.21-II.23 instead of the simple parabolic velocity profile used in the unidirectional flow study.

The channel height is fixed at 0.5 mm for this study (0.5 mm was the optimal value from the unidirectional flow results). The heat supplied to the SMA is varied, as is the oscillating Reynolds number (Re_W). The channel length to height ratio is 40. The fluid reservoirs are assumed to be maintained at 50° C.

The objective here again is to identify the flow conditions for which the greatest volume fraction that is transformed to both austenite (while heating) and martensite (while cooling). In other words, we want to design the system such that SMA is cooled in the fastest time possible to below the Martensite finish temperature after having been heated to above the Austenite finish temperature. The initial temeprature of both the fluid and the SMA is chosen such that the SMA is in the martensite form.

The plots shown in Figure II.13-II.15 are all for a frequency of actuation of 2 Hz. It is clear from Figure II.13 that the maximum output for a particular value of heat supplied to the SMA occurs at the maximum oscillating Reynolds number (which is proportional to A_o). This is however not the case in Figure II.14, because the higher flow frequency (ω) also contributes to a faster cooling time. The maximum volume fraction converted completely to martensite and austenite occcurs at a lower oscillating Reynolds number. This is seen to an extreme in Figure II.15, where ω = 10 Hz. The maximum volume fraction converted completely to martensite and austenite occcurs at the lowest oscillating Reynolds number. Comparison is made between the unidirectional flow and the oscillating flow results in Figure II.16. It is seen that the oscillating flow will produce an output that is 15% more than the unidirectional flow. However this doesn't consider

the extra energy that might be required to have an oscillating flow over an unidirectional flow of similar Reynolds number and also to maintain the fluid reservoirs at 50° C.

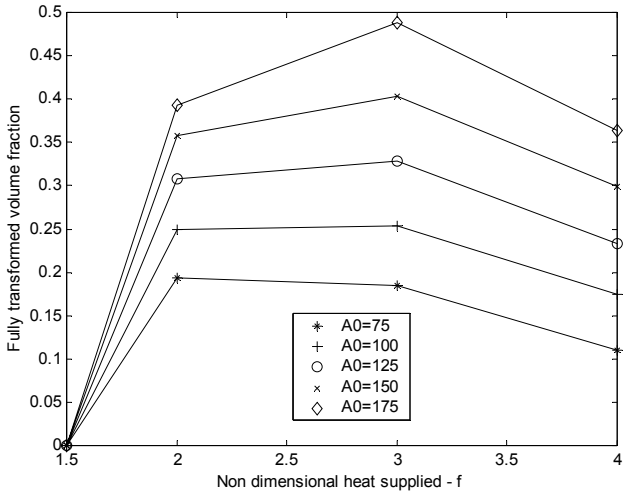

Figure II.13 $\omega = 4\pi$ rad/s, $T_E = 50$ C, $\Omega = 2\pi$ rad/s

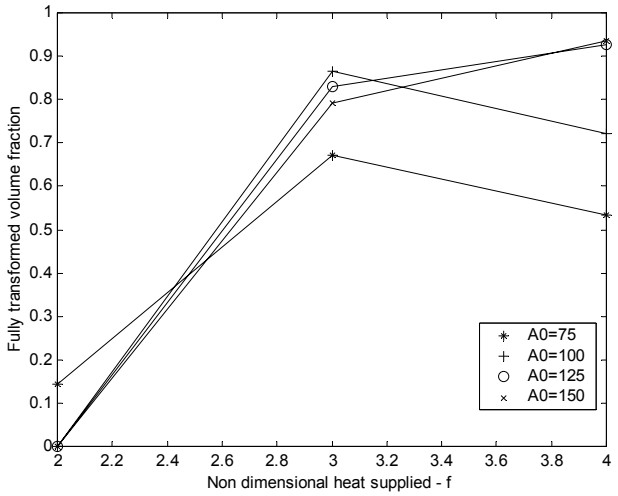

Figure II.14 $\omega = 10\pi$ rad/s, $T_E = 50$ C, $\Omega = 2\pi$ rad/s

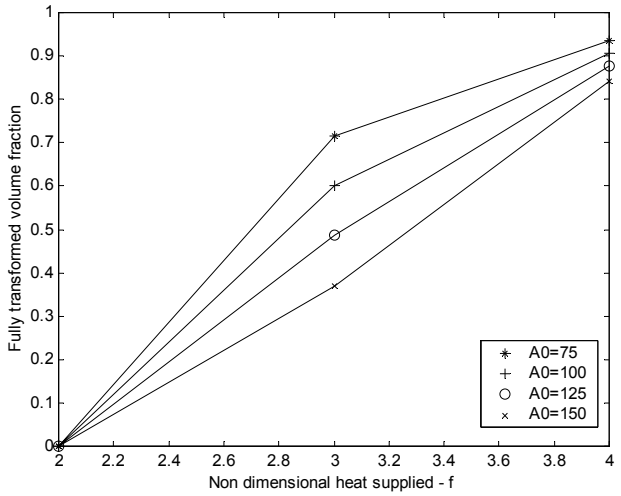

Figure II.15 $\omega = 20\pi$ rad/s, $T_E = 50$ C, $\Omega = 2\pi$ rad/s

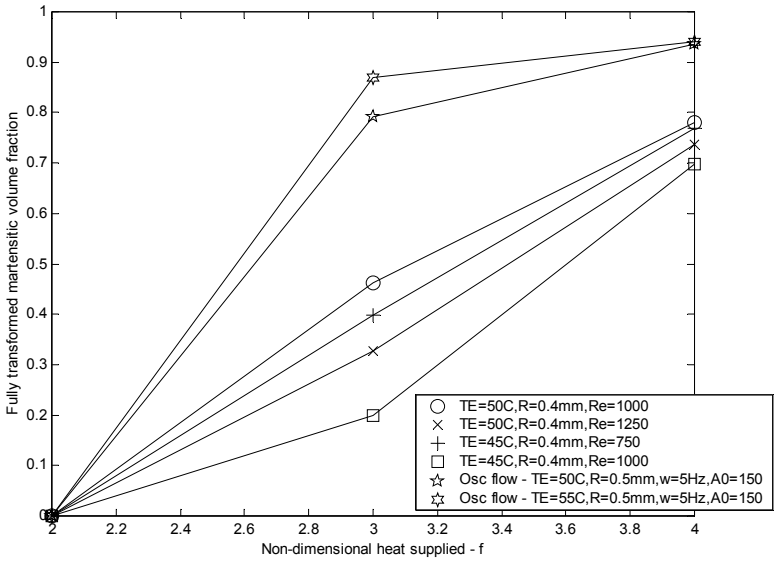

Figure II.16 Comparison between unidirectional and oscillating flow for $\omega = 1$ Hz

CHAPTER III
NUMERICAL SIMULATION OF OSCILLATING FLOW

Simulation of oscillating channel flow using SIMPLE

The analysis of the last section of Chapter II was based on an assumed velocity profile for the oscillating flow. It is however useful only for a preliminary analysis. In order to design an SMA actuator, a more accurate analysis is required and so the oscillating flow in a 2-D channel is simulated numerically using a finite volume method based on the SIMPLE (Semi Implicit Pressure Linked Equations) algorithm ([22] and [26]), which is used to couple the pressure and the velocities. This simulated velocity field will be used to solve the heat transfer problem of an SMA actuator. The domain is shown in the figure below.

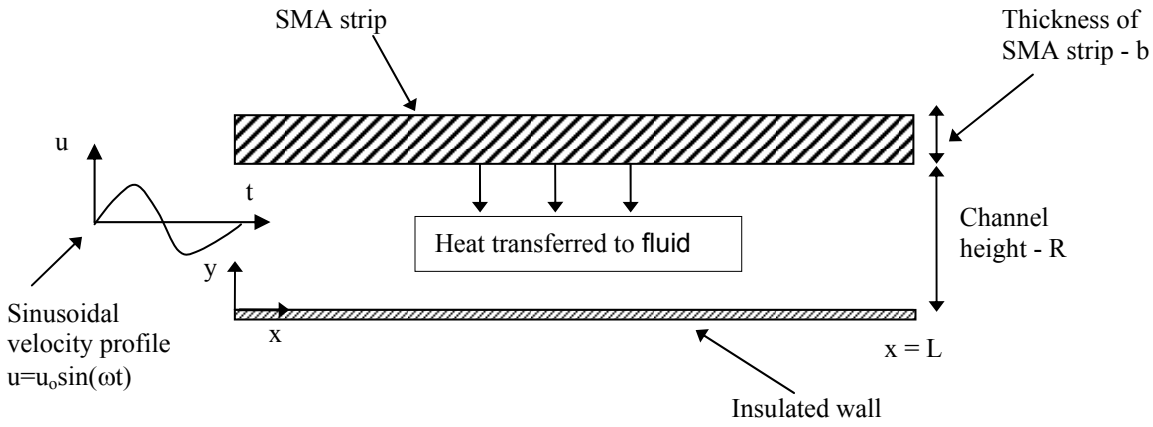

Figure III.1. Schematic of oscillating flow in a 2-D channel

The governing equations for the laminar, incompressible flow of a viscous fluid are the continuity equation

$$\frac{\partial u}{\partial x}+\frac{\partial v}{\partial y}=0\,, \tag{III.1}$$

the X-momentum equation

$$\frac{\partial u}{\partial t}+u\frac{\partial u}{\partial x}+v\frac{\partial u}{\partial y}=-\frac{1}{\rho}\frac{\partial p}{\partial x}+\nu\left(\frac{\partial^2 u}{\partial x^2}+\frac{\partial^2 u}{\partial y^2}\right) \tag{III.2}$$

and the Y-momentum equation.

$$\frac{\partial v}{\partial t}+u\frac{\partial v}{\partial x}+v\frac{\partial v}{\partial y}=-\frac{1}{\rho}\frac{\partial p}{\partial y}+\nu\left(\frac{\partial^2 v}{\partial x^2}+\frac{\partial^2 v}{\partial y^2}\right) \tag{III.3}$$

The boundary conditions (BC's) and the initial conditions (IC's) for the first half of the cycle are

$$u(o,y,t)=u_m\sin(\omega t),0<y<R,0<t\le\pi/\omega \tag{III.4}$$

$$v(o,y,t)=0,0<y<R,0\le t\le\pi/\omega \tag{III.5}$$

$$\frac{\partial u}{\partial x}=0,\frac{\partial v}{\partial x}=0-x=L,0<y<R,0\le t\le\pi/\omega \tag{III.6}$$

The BC's for the second half of a cycle are just reversed and the fluid enters the channel at x=L. The equations are solved using the SIMPLE algorithm on a staggered grid.

SIMPLE Algorithm

The staggered grid arrangement is shown above. It is used to avoid the so-called "Checkerboard" problem. The u and v velocity control volumes (CV) are displaced half a CV in the x and y directions respectively. The capital letters represent points where the variable is calculated. The small letters represent the faces of the control volume.

Consider the scalar ϕ and its flux, J, at the interfaces. J is defined as

$$J_X=\rho u\phi-\Gamma\frac{\partial\phi}{\partial x},J_Y=\rho v\phi-\Gamma\frac{\partial\phi}{\partial y} \tag{III.7}$$

This can be rewritten as

$$J^*=\frac{J\delta}{\Gamma}=P\phi-\frac{\partial\phi}{\partial(x/\delta)}=P\phi-\frac{\partial\phi}{\partial x^*} \tag{III.8}$$

Where $P = \frac{\rho u \delta}{\Gamma}$ and $x^* = \frac{x}{\delta}$ and δ is the grid size.

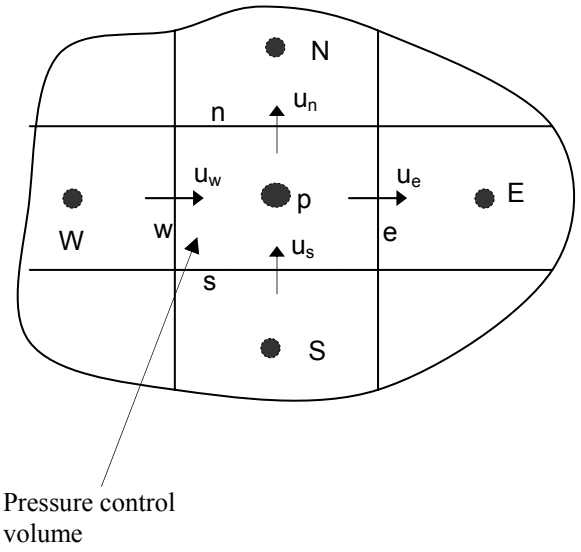

Figure III.2. Pressure control volume

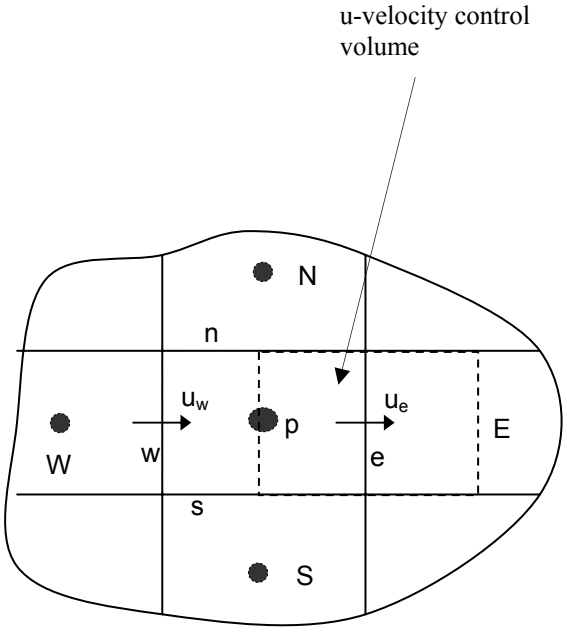

Figure III.3. u-velocity control volume

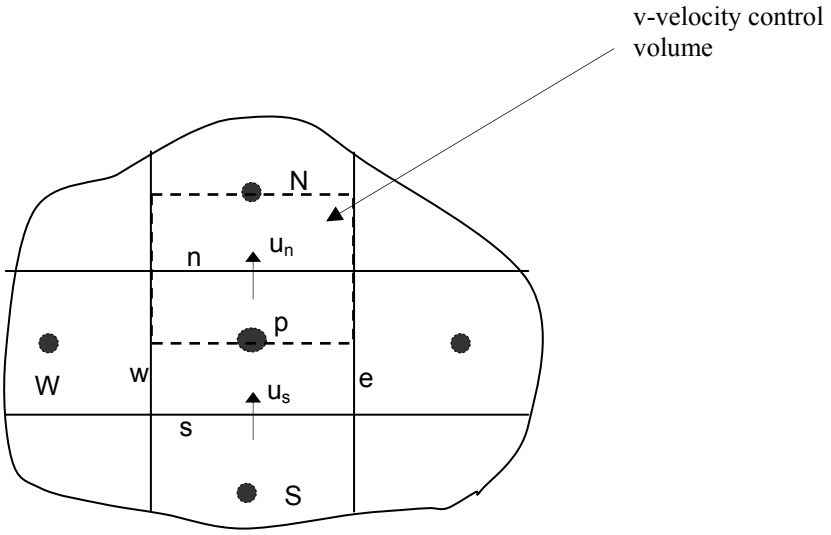

Figure III.4. v-velocity control volume

At the interface of two control volumes the value of ϕ is assumed to be some weighted average of the value at the grid points inside the two control volumes, while the gradient is taken to be proportional to the difference in the value of ϕ at the two grid points inside the control volumes under consideration (ϕ_{i+1}-ϕ_i). This is written as

$$\phi_{\text{int}erface} = \alpha\phi_i + (1-\alpha)\phi_{i+1} \quad \text{and} \quad \left.\frac{\partial\phi}{\partial x^*}\right|_{\text{int}erface} = \beta(\phi_{i+1} - \phi_i) \tag{III.9}$$

Where α and β are functions of P. This reduces to the form $J^* = B\phi_i - A\phi_{i+1}$. It can be shown that $B = A + P$.

Now for the conservation of ϕ, the sum total flux of ϕ in the x direction, the flux in the y direction, the source (or sink) contribution inside the control volume must be a constant. This implies that

$$\frac{\partial(\rho\phi)}{\partial t} + \frac{\partial J_X}{\partial x} + \frac{\partial J_Y}{\partial y} = S \tag{III.10}$$

Setting ϕ = u and $S = -\frac{\partial p}{\partial x}$ generates the u momentum equation. We can generate the v momentum b setting ϕ = v and $S = -\frac{\partial p}{\partial y}$. Here S is similar to a source term.

Integrating (39) over the control volume we get,

$$\rho(\phi^n - \phi^{n-1})\Delta V/\Delta t + J_e - J_w + J_n - J_s = S_{avg}\,\Delta V \qquad \text{(III.11)}$$

where n and (n-1) represent the current and previous time levels, S_{avg} is the average value of S over the control volume and ΔV is the volume of the control volume and is equal to ($\Delta x * \Delta y$) for the 2-D case.

There are many models for A and B as functions of P and the model used here is the Power law method of Patankar [22]. According to this model

$$A(|P|) = \max\left(0, (1 - 0.1|P|)^5\right) \text{ for } |P| \le 10 \qquad \text{(III.12)}$$

$$A(|P|) = 0, \text{ otherwise}$$

This reduces the integrated momentum equation to the form

$$a_P u_P = a_E u_E + a_W u_W + a_N u_N + a_S u_S + b + A_P(P_P - P_E) \qquad \text{(III.13)}$$

where

$$a_E = D_e A(|P_e|) + \max(-F_e, 0), a_W = D_w A(|P_w|) + \max(F_W, 0), a_N = D_n A(|P_n|) + \max(-F_n, 0)$$

$$a_S = D_s A(|P_s|) + \max(-F_s, 0), a_P = a_E + a_W + a_N + a_S + a_P^o$$

$$b = a_P^0 \phi^{n-1}, a_P^o = \frac{\rho \Delta V}{\Delta t}$$

and $D_e = \frac{\Gamma \Delta y}{\delta x_e}, F_e = (pu)_e etc$

In the above, F is any flow variable or mass of fluid flowing into or out of the CV through the face of the CV and ΔV is the volume of the CV. We get an equation similar to (42) for each CV.

Now we have to solve (42). If we use an explicit method for time stepping, we have just one variable. This means we assume an initial value for all u's and then get u at every point by calculating the coefficients and substituting into (38). We have to keep

doing this iteratively till we reach some kind of convergence, absolute or relative. However the explicit method is highly unstable and requires a very small time step and it is computationally prohibitive to use for large problems or problems with a large number of CVs.

An alternative is to use an implicit method. We use a staggered grid to avoid what is known as checkerboard oscillation. If we use a non-staggered grid, then a wavy velocity or pressure field may be sensed as a uniform field. So we have to use a staggered grid where u, v and p are calculated at different points as shown in Figure III.2 - Figure III.4.

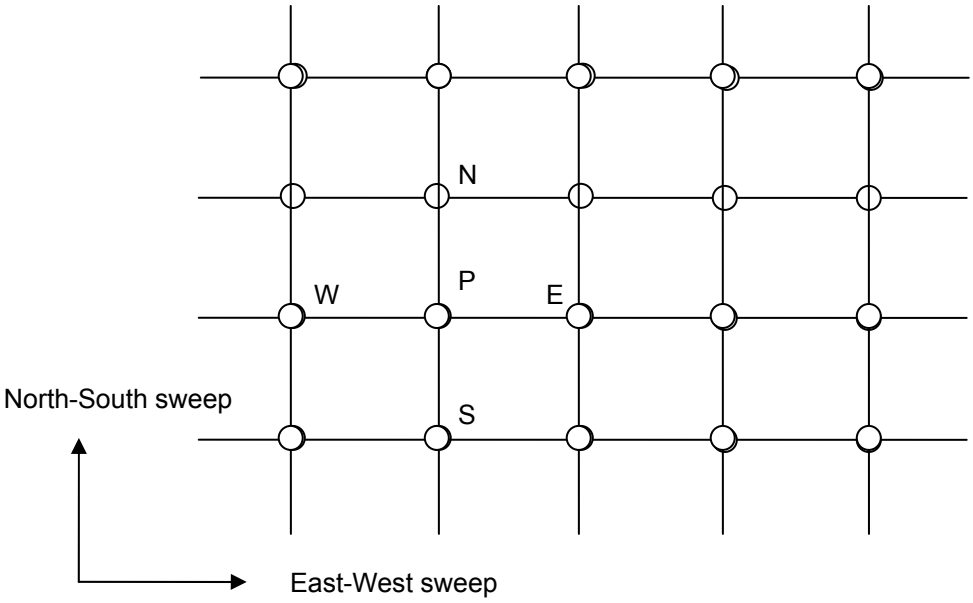

Figure III.5. Line-by-line method

Now (42) has 5 variables. When the matrix is setup for solving the entire domain, a pentadiagonal matrix emerges and it is hard to solve. So a line-by-line iterative method is used wherein the equation for each node has 3 unknown rather than 5. For example, in Figure III.5, W, P and E become the variables and N and S are assumed to be known and then equation is setup. We setup the equations for all points along a West-East line. In this case we get a tridiagonal matrix and it can be easily solved using the Thomas

algorithm. So each East-West line is solved and this constitutes a North-South sweep. Now we go line-by-line in the North-South or South-North direction and complete an East-West sweep. In this case, we look at lines going from north to south and have N, P and S as variables and W and E as known quantities.

It is imperative we use some relaxation to prevent instability in the numerical procedure.

So for a West-East line, we have

$$-a_W u_W + \frac{a_P}{\alpha_u} u_P - a_E u_E = a_N u_N + a_S u_S + a_P(\frac{1}{\alpha_u} - 1)u_P^0 + b + A_P(P_P - P_E) \quad \text{(III.14)}$$

where u_P^0 is the velocity at point P from the previous time step and α_u is the under-relaxation factor(<1) for u. Similarly for a North-South line we have

$$-a_S u_S + \frac{a_P}{\alpha_u} u_P - a_N u_N = a_W u_W + a_E u_E + a_P(\frac{1}{\alpha_u} - 1)u_P^0 + b + A_P(P_P - P_N) \quad \text{(III.15)}$$

The pressure difference ($P_P - P_E$) or ($P_P - P_N$) drives the flow within each control volume. We can solve similarly for v.

The solution procedure is started by assuming an initial solution for u, v and p and then solving for u and v as shown above. Since what we get from the above formulation is an approximation, u^*, let us take the actual velocity to be

$$u = u^* + u^1 \quad \text{(III.16)}$$

where u^1 is a correction to u^*.

The velocity field is governed by

$$a_P u_P = \sum a_{nb} u_{nb} + b + A_P(P_P - P_E) \quad \text{(III.17)}$$

Here nb represents the surrounding four points, namely n, s, e and w.

The velocity field due to a guessed pressure field P^* is governed by

$$a_P u_P^* = \sum a_{nb} u_{nb}^* + b + A_P(P_P^* - P_E^*) \quad \text{(III.18)}$$

Subtracting (47) from (46) we get an equation for the velocity correction.

$$a_P u_P^1 = \sum a_{nb} u_{nb}^1 + A_P(P_P^1 - P_E^1) \quad \text{(III.19)}$$

If we solve for the velocity correction as such we will again have a pentadiagonal matrix. This is very difficult to solve. Since this is an iterative method, the contribution of velocities of neighbouring nodes in (48) is neglected to get an explicit expression for the velocity correction in terms of the pressure correction. When the iteration for the current time step converges, the velocity corrections will anyway be zero and won't contribute anything to the above equation. This is the reason why the method is semi-implicit and not fully implicit.

So we have

$$u_p^1 = \frac{A_P}{a_p}(P_P^1 - P_E^1) = d_p(P_P^1 - P_E^1) \qquad \text{(III.20)}$$

Substituting $\phi = 1$ in (39) and integrating over the CV gives the discrete form of the continuity equation to be

$$[(pu)_e - (pu)_w] * \Delta y + [(pu)_N - (pu)_S] * \Delta x = 0 \qquad \text{(III.21)}$$

If we substitute $u=u^*+u^1$ and take u^* as a known quantity and substitute for u^1 from (49), we get an equation for P^1.

$$a_P P_P^1 = a_W P_W^1 + a_E P_E^1 + a_S P_S^1 + a_N P_N^1 + [(pu^*)_e - (pu^*)_w] * \Delta y + [(pu^*)_N - (pu^*)_S] * \Delta x \qquad \text{(III.22)}$$

We have to solve this equation in a line by line manner as was done for the u and v velocities. Once p^1 has been calculated, we can get the velocity corrections using (49). There we correct the velocities using $u=u^*+u^1$ and pressure as $p = p^* + \alpha_P p^1$ where α_P is the under relaxation factor for pressure.

Then we check for convergence using some residual such as

$$R_u = \sum | a_p u_p - \sum a_{nb} u_{nb} - A(P_P - P_E) | \quad \text{(Absolute convergence)} \qquad \text{(III.23)}$$

or

$$R_u = \frac{\sum | a_p u_p - \sum a_{nb} u_{nb} - A(P_P - P_E) |}{\sum | a_p u_p |} \quad \text{(Relative convergence)} \qquad \text{(III.24)}$$

The code was tested for the case of a unidirectional channel flow. If the inlet velocity to the channel is u_m, then the center velocity at the exit must be $1.5u_m$.

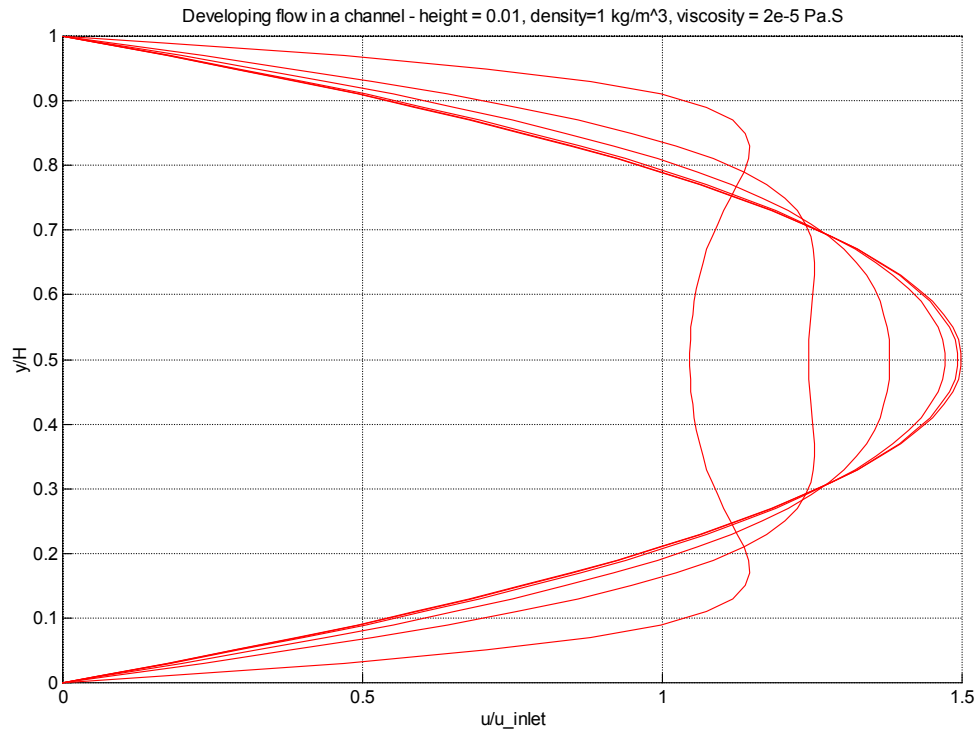

Figure III.6. Channel flow steady state velocity profiles at various axial locations

The Figure III.6 shows velocity profiles at different locations in the channel. The value of u/u_inlet is 1.449 at the center (y = 0.5) of the channel at the exit. The exact value is 1.5 and so the error is less than 0.1 %.

Then the code was tested for the case of an oscillating flow. Two values of the oscillation frequency are plotted. At low frequencies, the velocity profiles are well developed in the bulk of the fluid. At high frequencies, the bulk fluid is more or less a plug flow. The plots shown are for ω = 4 Hz (8π rad/s) in and ω = 10 Hz (20π rad/s) in Figure III.7 and III.8.

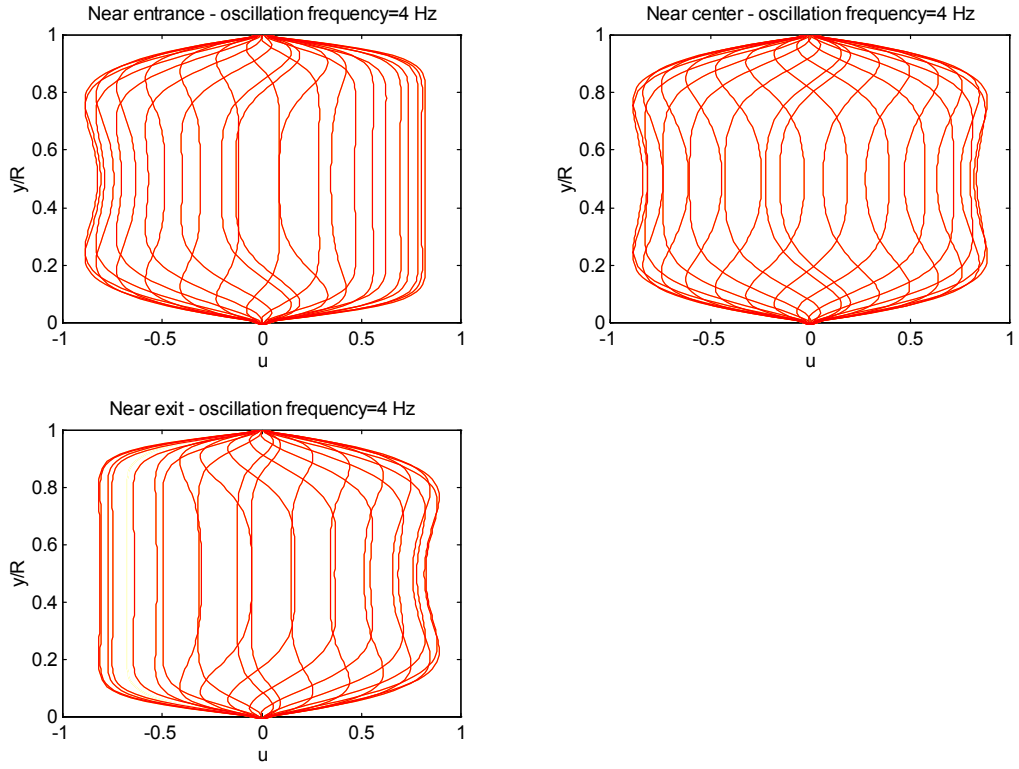

Figure III.7 Oscillating flow at ω = 4 Hz

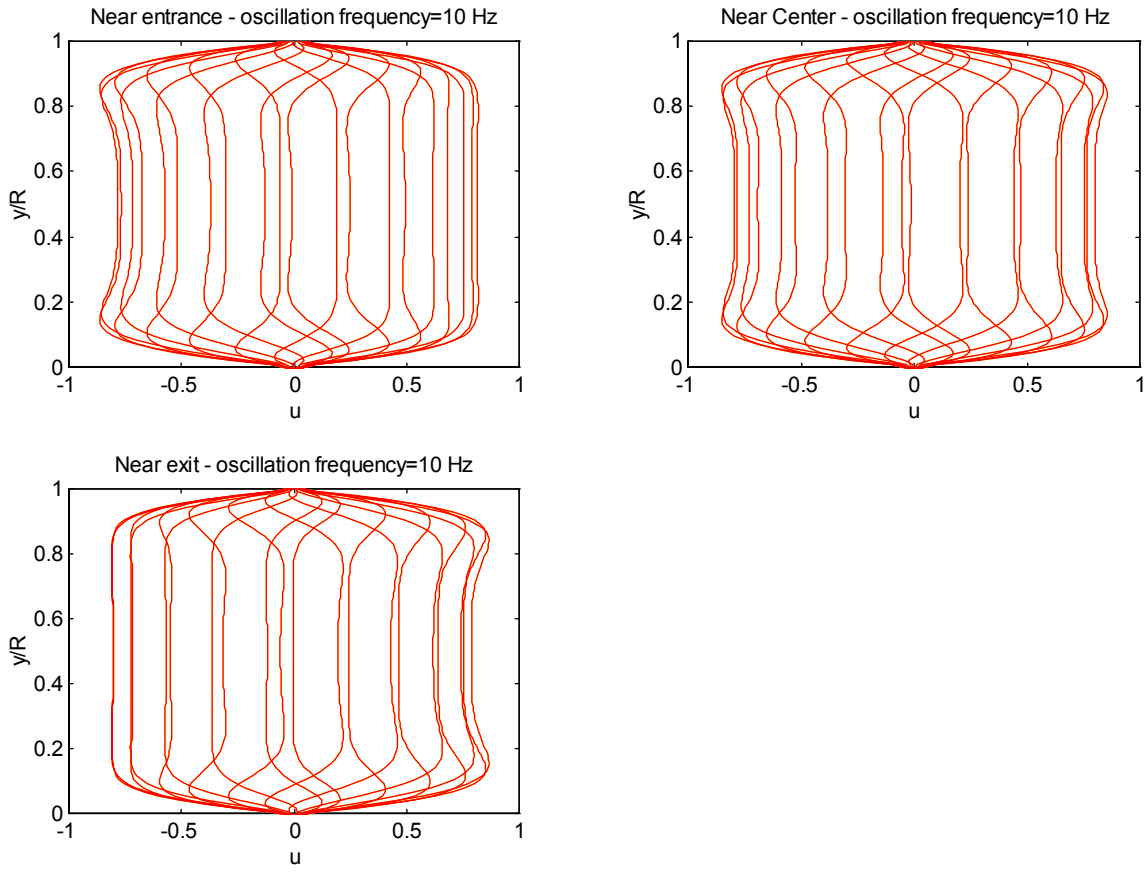

Figure III.8 Oscillating flow at ω = 10 Hz

The code is tested by comparison with a known analytical solution of a simplified problem. The first quarter of a cycle is show in Figure III.9. The fluid is being pushed from the left to the right. Fluid near the channel walls has a higher velocity than at the center of the channel and is still traveling towards the left reservoir even as the fluid at the center has already reversed direction.

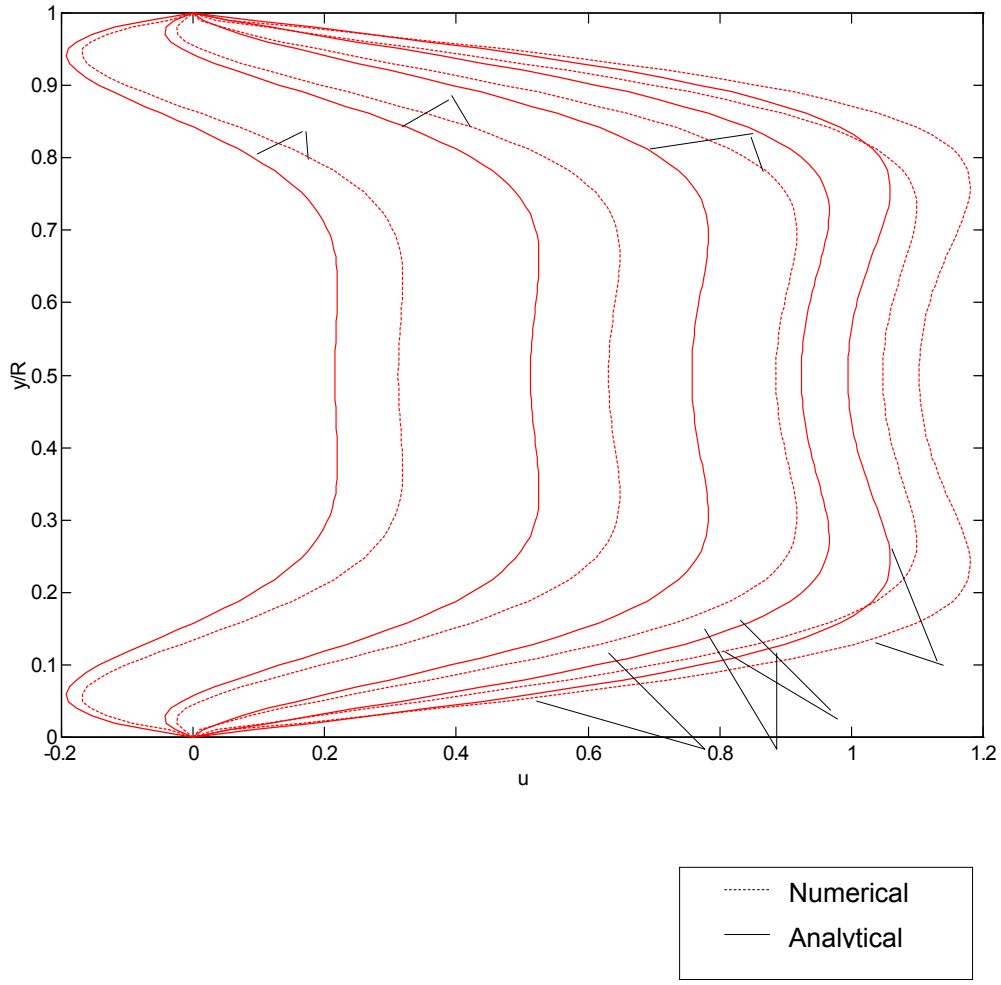

Figure III.9. Comparison of code with theoretical solution for ω = 5 Hz

The second quarter of a cycle is shown in Figure III.10. The difference between the analytical and numerical solution maybe due to inlet and exit effects ([16]).

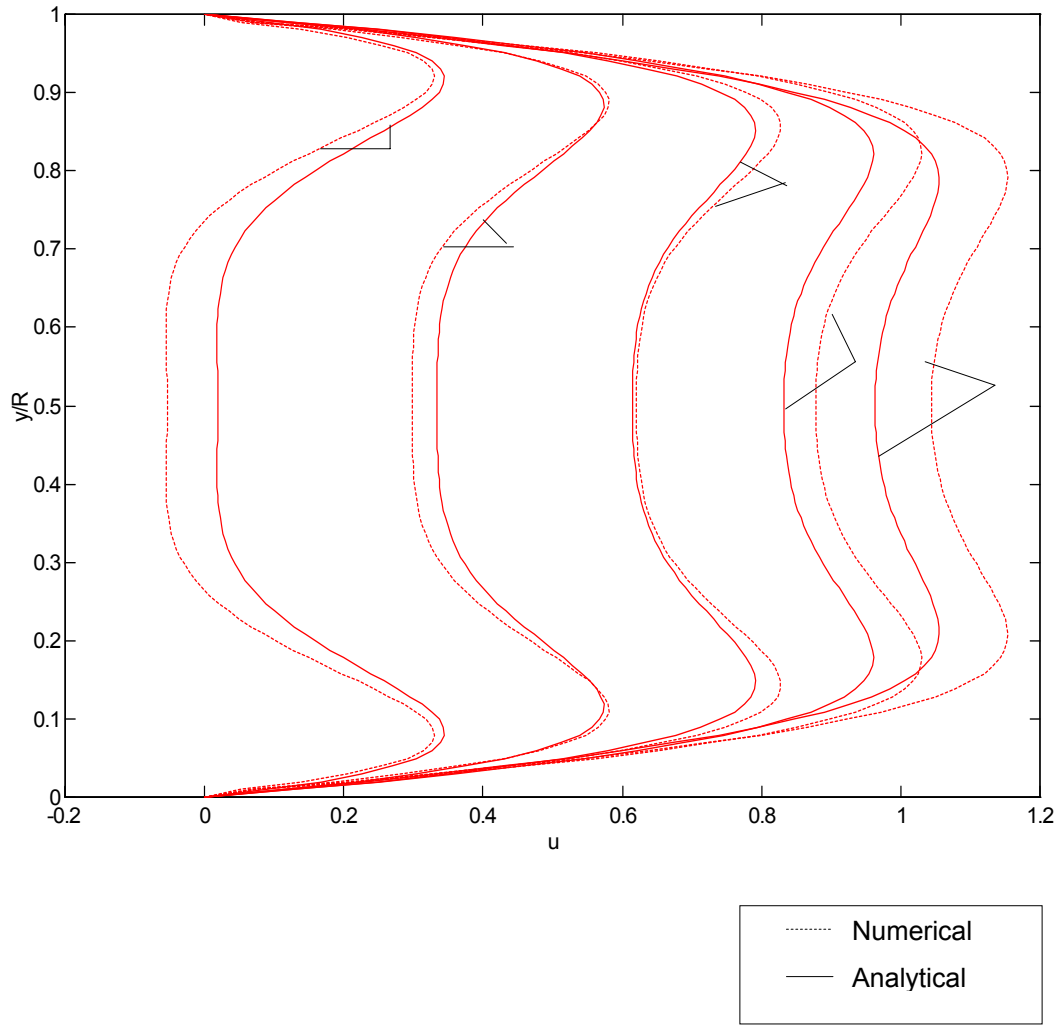

Figure III.10. Comparison of code with theoretical solution for ω = 5 Hz

Now the energy equation solver (described in the appendix) was tested. For a unidirectional flow in a channel with uniform heat flux from both walls the Nusselt number asymptotically reaches a value of 7.54. The code used here gives a value of 7.43, an error of 1.5%.

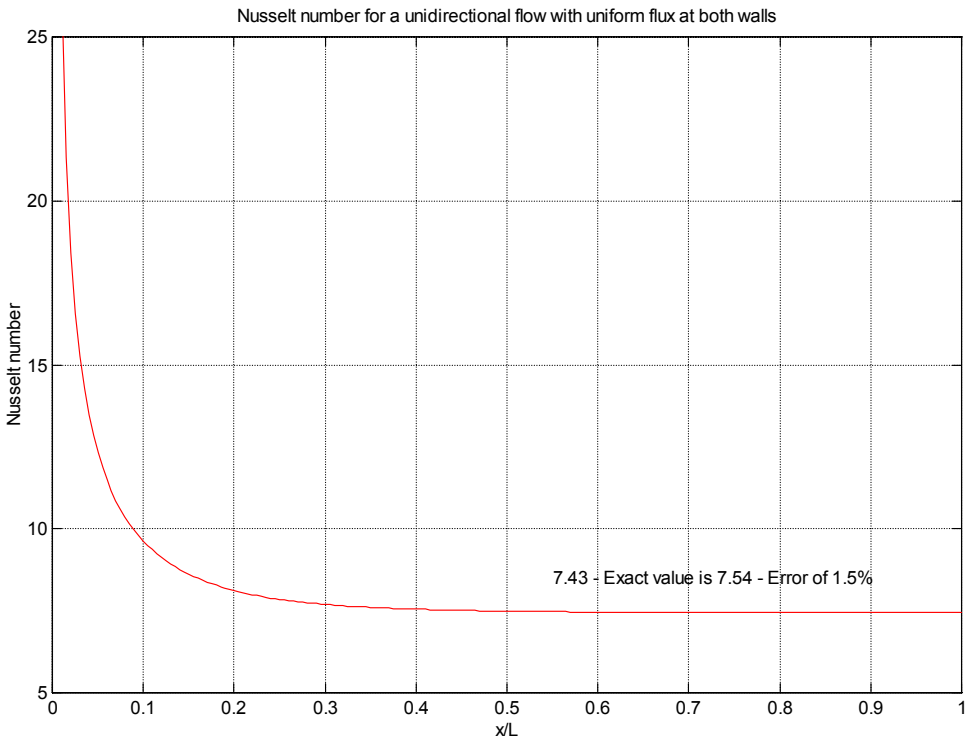

Figure III.11. Nusselt number for uniform wall flux problem

Nusselt number for oscillating flow

The instantaneous Nusselt number for the oscillating flow at any axial location is defined as

$$Nu(x,t)=\frac{2}{\theta_w(x,t)-\theta_b(x,t)},\theta_b(x,t)=\frac{\int_0^R \theta(x,y,t)\left|u(x,y,t)\right|dy}{\int_0^R \left|u(x,y,t)\right|dy} \qquad \text{(III.25)}$$

The usual definition of Nusselt number fails when applied to oscillating flow, producing unnatural Nusselt numbers. So it is changed slightly, with the use of the absolute value of the flow velocity, to account for flow reversal.

CHAPTER IV

RESULTS

A parametric study was conducted to identify the flow conditions that would produce the maximum output from the SMA actuator. The parameter space allows us to control both the geometry of the actuator and also the flow conditions. The parameter space includes

1) Channel height - R
2) Thickness of the SMA strip - b
3) Entry temperature - T_E
4) Flow oscillation frequency - ω_f
5) Actuation frequency - ω_a
6) Tidal displacement – A_0 ($\Delta x/R$)
7) Heat supplied to the SMA strip

The parameter Δx, the tidal displacement (A0 = non-dimensional tidal displacement = Δx / R), represents the average distance traveled by any particle within the channel in a half-cycle. So if the tidal displacement is chosen to be less than L/2 (L = length of channel), then there will be a significant portion of the fluid, which is inside the channel at the start of the cycle, which will still be inside the cycle at the end of a half cycle. So this portion of the fluid will never leave the channel and mix with the colder fluid in the reservoir. So the temperature of this part of the fluid inside the channel will keep increasing monotonously. As a result a significant portion of the SMA will never be cooled adequately.

In some cases it might be necessary to choose a value of Δx less than half the channel length. In such a situation there is no net transfer of fluid from the channel to the reservoir. This is the case in nuclear reactors [30]. However in this study we want the heated fluid from the channel to reach the reservoir. So A_0 will be chosen to be greater

than 0.5* L/R i.e. $\Delta x \geq L/2$. A smaller value of Δx will be chosen to show that it does indeed cause decrease the effectiveness of the cooling.

With such a large number of parameters affecting the flow and the heat transfer, it is imperative to fix certain parameters. The SMA strip thickness is first fixed at 0.5 mm i.e. $5*10^{-4}$ m. The SMA strip thickness was selected to satisfy actuator force output requirements. Next the channel height is initially fixed at 1.5mm. Also the entry temperature of the fluid is fixed at 50° C. Also the actuation frequency, ω_a, is fixed at 2 Hz (or 4π rad/s).

So the parameters that are initially varied are the oscillation frequency (ω_f), tidal displacement (A_0) and the heat supplied to the SMA (f). The parameter space under study is shown in Table IV.1.

Table IV.1. Parameter Space

ω_f /2*π (Hz)	A_0	f
5	50	10,14,17,20
5	60	10,14,17,20
5	70	10,14,17,20
10	50	10,14,17,20
10	60	10,14,17,20
10	70	10,14,17,20

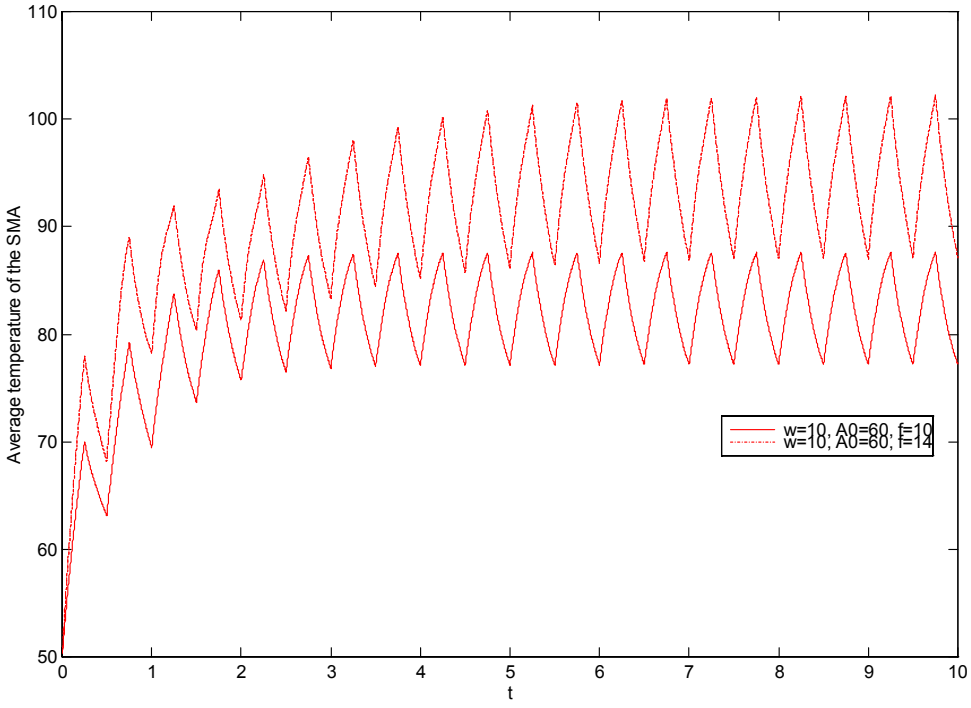

Figure IV.1. Comparison of average SMA strip temperature for 2 values of f

Figure IV.1 shows that as heat supplied is increased the average temperature value increases rapidly and the flow is not able to cool it. During heating, there is a resistance to the increase of temperature because of the latent heat of transformation. This quantity of heat has to be supplied to the SMA to change into Austenite. The Austenite transformation temperatures are A_s = 71.0° C and A_f = 98.0° C. During the cooling part, the latent heat of transformation has to be removed from the SMA.

It is clear from the Figure IV.2 that for f = 8 the SMA undergoes complete transformation to austenite (during heating) and to martensite (during cooling). Therefore an actuator frequency of 1 Hz is achieved.

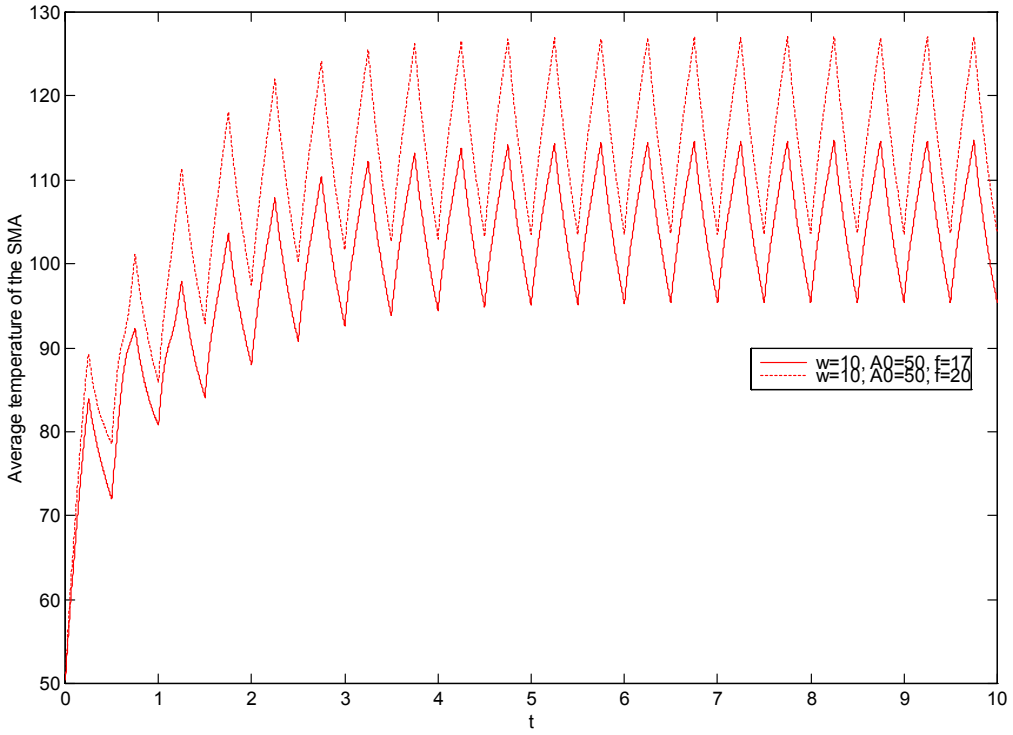

Figure IV.2 Average wall temperature for Ω = 1 Hz

From Figure IV.3 we can see that the SMA is being heated up very quickly and that the cooling provided by the oscillating flow is not enough. Average temperatures at the end of the cooling period are still greater than 90° C.

In Figure IV.4 we can see that the entire SMA is undergoing complete transformation to austenite during heating and most of the SMA is transformed back to martensite completely at the end of the cooling period. At the end of the cooling cycle, the SMA temperature near the center of the channel (where the temperature should be highest) is about 73° C, which is just above the Martensite finish temperature of 71° C.

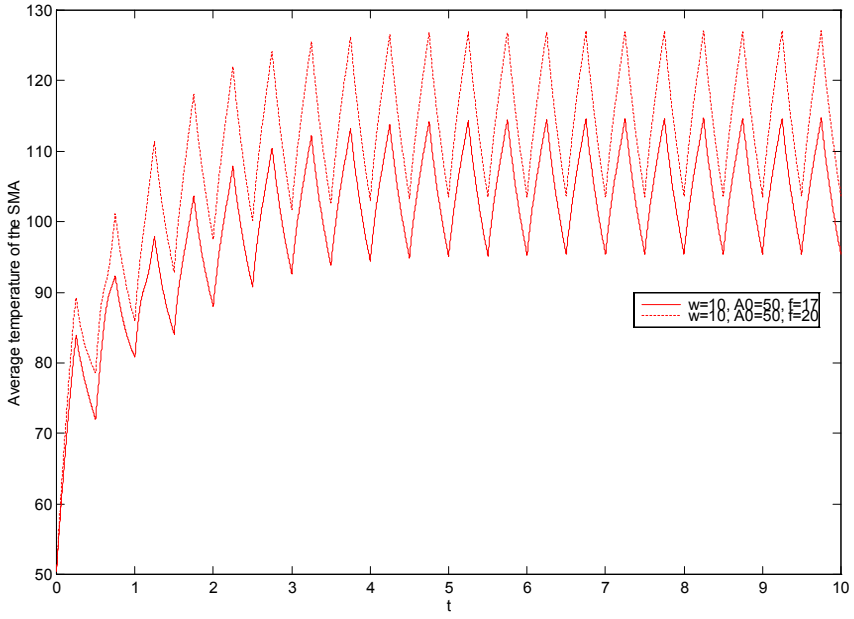

Figure IV.3. Comparison of average SMA strip temperature for 2 values of f

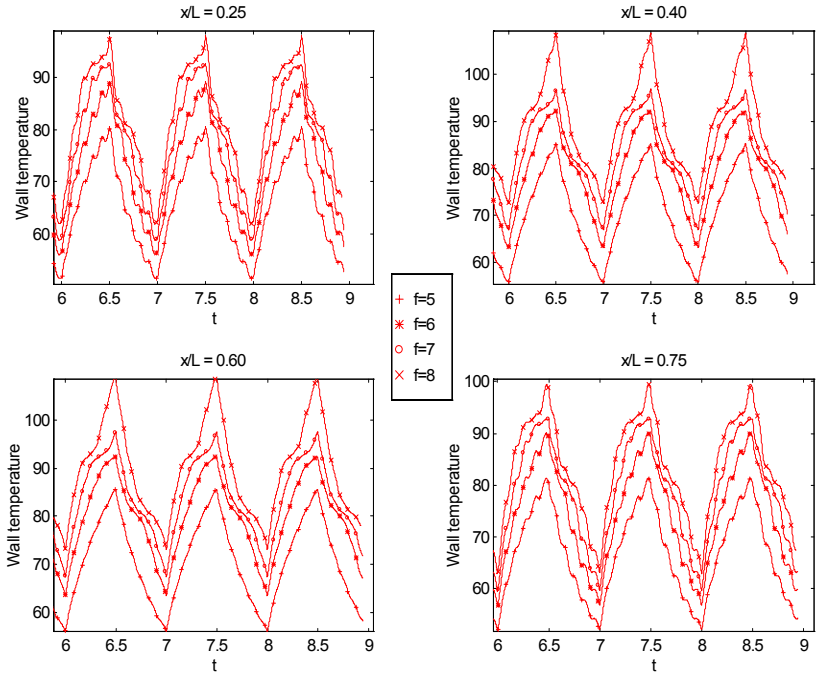

Figure IV.4. Comparison of wall temperatures for flow frequency of 10 Hz

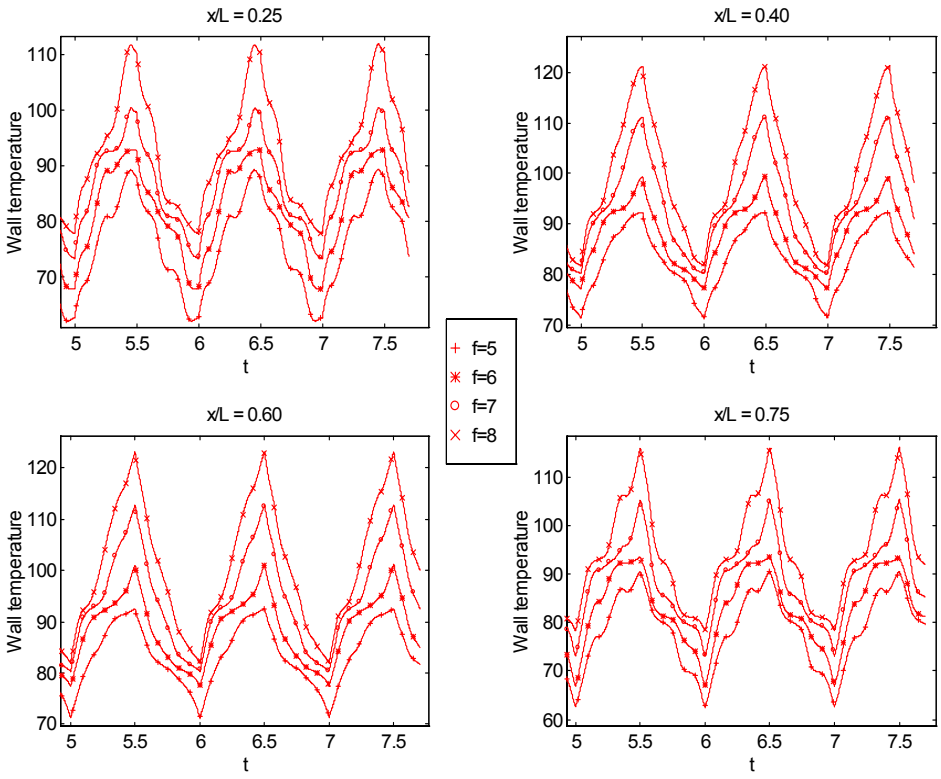

Figure IV.5. Comparison of wall temperatures for flow frequency of 5 Hz

Figure IV.5 and Figure IV.6 are for a flow frequency of ω = 5 Hz. We can from Figure IV.6 that the SMA is completely transformed to austenite, after the heating half of the cycle (with an average temperature greater than 98° C) and to martensite, after cooling (with an average temperature less than 71° C), for both f = 7 and 8.

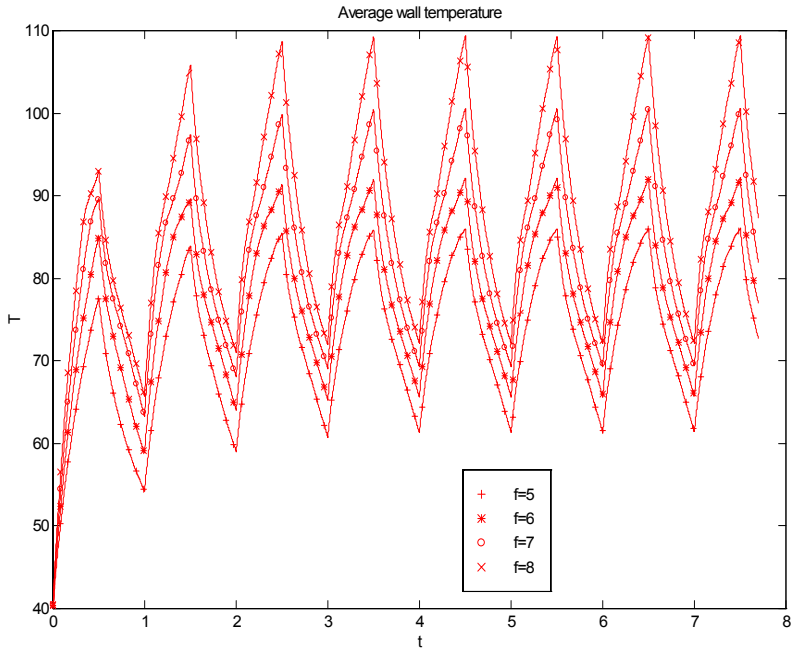

Figure IV.6. Comparison of average wall temperatures for flow frequency of 5 H z

From Figure IV.7 we can see that the temperature after the cooling half of the cycle is over is still much higher than the martensite finish temperature of 71° C, so that there is no complete transformation to martensite after the cooling phase. This is even clearer from Figure IV.8.

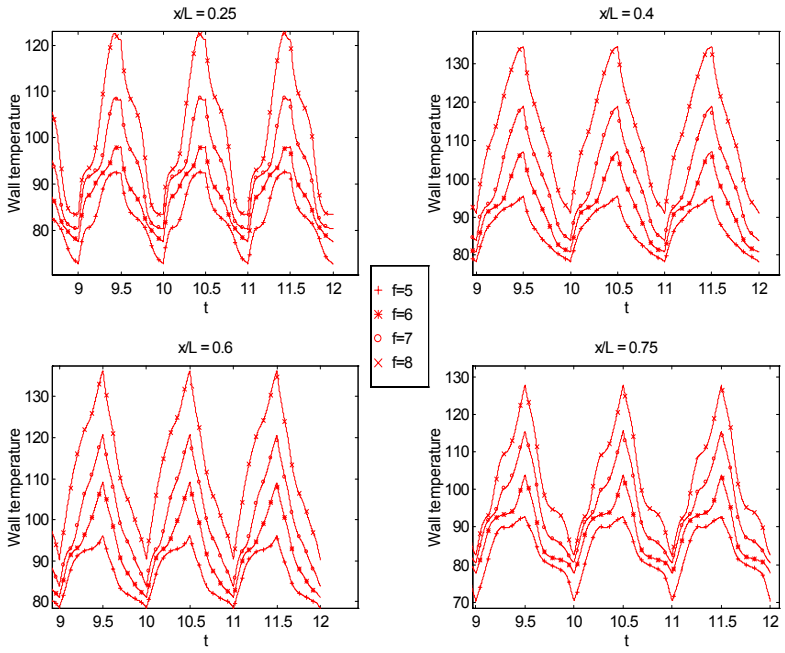

Figure IV.7. Comparison of wall temperatures for a flow frequency of 3Hz

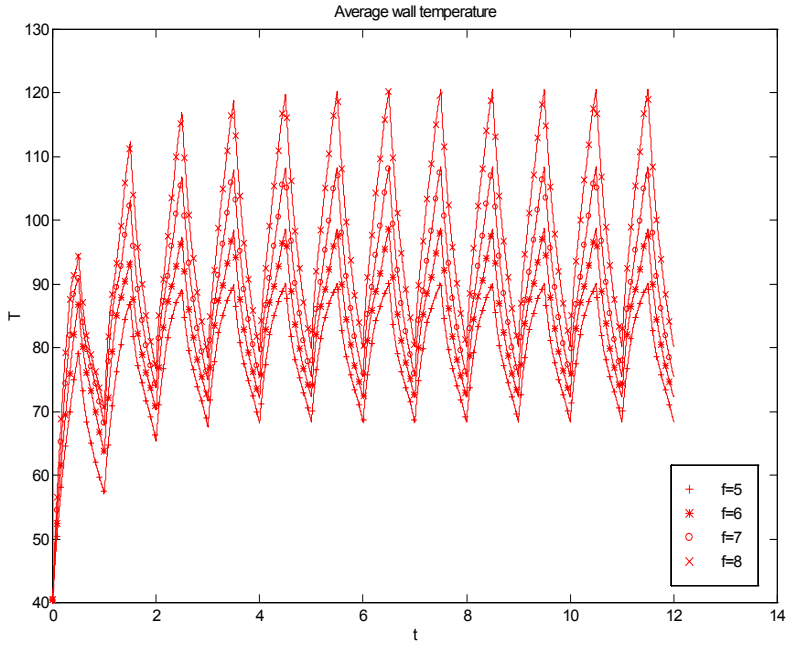

Figure IV.8. Average wall temperatures for flow frequency of 3Hz

The Nusselt number for a unidirectional flow with one wall of the channel insulated and other wall having uniform flux reaches an asymptotic value of 5.39. This study is similar to the above mentioned unidirectional flow case but the heat flux in this study is a varying quantity. If the oscillating flow were to be more effective than the unidirectional flow, then the average Nusselt number in the oscillating flow case should be higher than this value of 5.39.

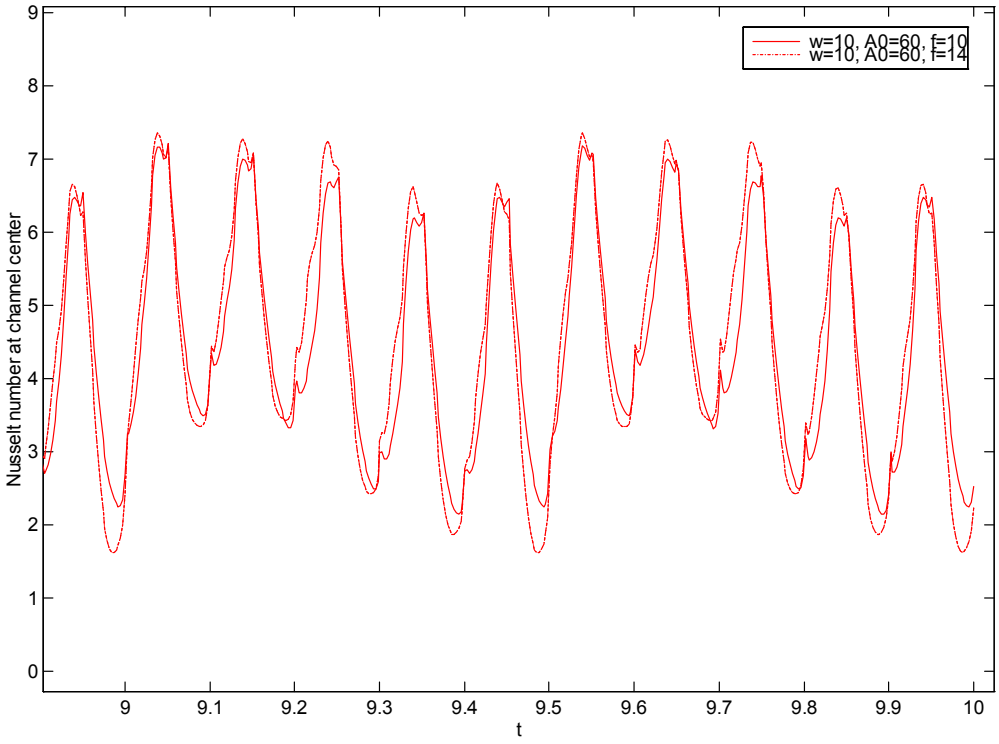

Figure IV.9. Nusselt number variation for two different values of heat supplied

The Nusselt numbers for the 2 cases plotted are very close because the flow parameters do not change. Only the heat supplied to the SMA changes. This is more clearly seen in Figure IV.1. The time-averaged Nusselt number for the two cases in Figure IV.9 is less than less than the unidirectional steady flow value of 5.39. The actuation frequency is fixed at 2 Hz. This means that heat is supplied to the SMA from N

to (N+0.25) seconds and from (N+0.5) to (N+0.75) seconds where N is any integer. From (N+0.25) to (N+0.5) and from (N+0.75) to (N+1) there in no heating and so the flow tries to cool the SMA strip. Since flow oscillation frequency, ω_f, is 10 Hz, this means that during the cooling portion [(N+0.25) to (N+0.5) and from (N+0.75) to (N+1) seconds] there are more than 2 flow reversals and that is why the Nusselt number plot show a periodic rise and fall.

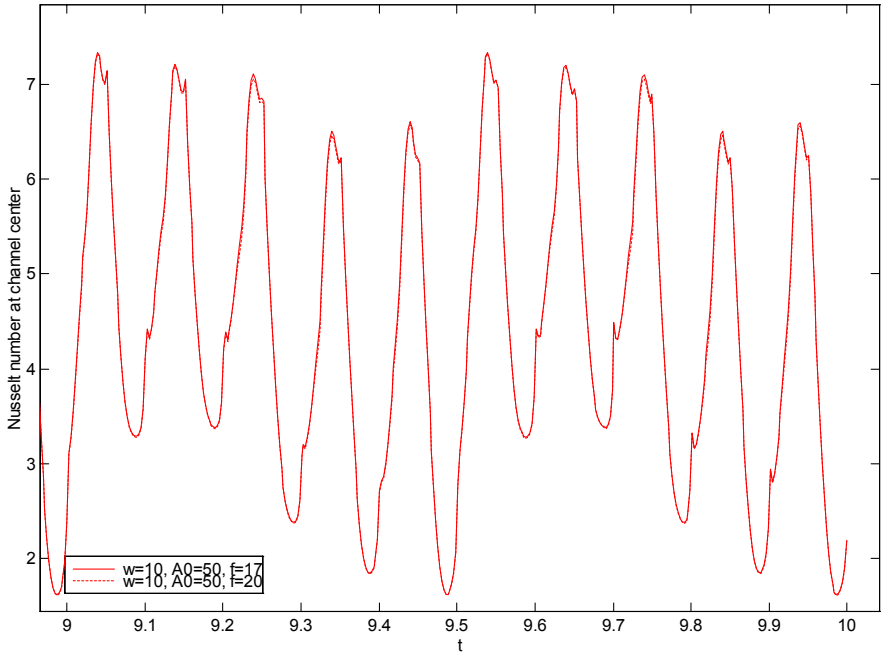

Figure IV.10. Nusselt number for 2 different values of heat supplied

In Figure IV.10 and Figure IV.3 a lower value of A_0 (50) is used and the heat supplied are also increases to 17 and 20. We can see that it is the flow parameters that determine the Nusselt number rather than the value of the heat flux. The 2 Nusselt number plots are identical. Figure IV.3 shows that average temperature has increased enormously and that the SMA is not being cooled fast enough. It may be due to the decreased value of A_0 or the frequency of oscillation could be too high. So it needs to be compared with a lower value of frequency with everything else remaining the same.

CHAPTER V

CONCLUSIONS

Heat transfer analysis of a convection cooled SMA was undertaken. First a uniform one directional flow was assumed in the channel and the SMA was heated periodically. With a number of parameters affecting the flow and the heat transfer, some were held fixed to reduce the parameter space under study. The output of the SMA actuator, which is directly proportional to the volume of SMA which undergoes complete transformation to Austenite during heating and to Martensite under cooling, is the main quantity of interest in all the simulations.

Supplying too much heat means more heat needs to be removed during the cooling phase. On the other hand not supplying enough heat for a given flow condition means that the SMA is not heated enough to attain complete transformation to Austenite. The goal is then to find an optimum flow rate and heat supply to maximise the volume undergoing complete transformation.

For the uniform flow case it was found that at optimum conditions, 80% of the SMA could undergo complete transformation (Figure II.5). The volume undergoing complete transformation is a non-linear function of the channel height for fixed Reynolds number and heat supply.

Next an oscillating flow was considered. The analysis is carried out as before by using a known analytical velocity profile for oscillating flows. In this case there is an additional variable to be considered, namely, the frequency of oscillation of the flow. The volume of SMA undergoing complete transformation was found to be a nonlinear function of the heat supplied. This is to be expected because beyond a certain point the flow cannot remove any more heat and the SMA cannot be cooled beyond a certain point for any flow condition.

The oscillating flow was then simulated using a finite volume code and the heat transfer analysis was repeated. The SMA strip thickness, the channel height,

entry/reservoir temperature of the fluid and frequency of actuation were fixed. The heat supplied the frequency of oscillation of the flow and the tidal displacement (related to the Reynolds number of the flow) was varied. The entire SMA was found to undergo complete transformation for a flow frequency of 5 Hz (Figure IV.6).

While direct comparison with uniform flow has not yet been done, the Nusselt number was calculated (Figure IV.1, Figure IV.9). The average Nusselt number was found to be less than the value for uniform flow. This indicates that in the parameter space under study, the uniform flow is better at removing heat from the SMA than the oscillating flow.

Limitations of the study

1) While the flow problem is 3-D, it was assumed that a 2-D simulation would suffice. Further investigation needs to be done to see if there 3-dimesnional effects affecting the flow, and hence the heat transfer, differently.
2) In the oscillating flow simulation, the heated fluid exits the channel into the reservoir and is assumed to re-enter the channel at the same temperature that it exited at.. To account for mixing in the reservoir, the flow in the reservoir also needs to be simulated and it was beyond the scope of this thesis. This is an area where further work is needed.
3) Axial conduction terms in the energy equation were neglected because the Biot number was found to be small. This should be investigated in future works.
4) The boundary conditions for the SMA strip temperature were assumed to be zero gradient.
5) Nusselt number definition for the oscillating flow are not agreed upon in literature and the proper form of the Nusselt number definition needs to used to facilitate comparison with the Nusselt number from unidirectional flow.

6) The cooling fluid was taken to be water throughout the study. Other cooling fluids with better properties (low viscosity and density and high thermal conductivity) need to be investigated.

   Also, the bulk temperature of the fluid crosses 100° C in certain cases. So boiling of the fluid needs to be taken into account under such circumstances.

While the unidirectional flow was found to be more effective than the oscillating flow in the parameter space studied, we believe a bigger parameter space will show that the oscillating flow can be a more effective cooling environment for SMA actuators than the unidirectional convection. The oscillating flow showed a definite improvement over the uniform flow (Figure II.16) for certain values of the parameters. The entire SMA was found to undergo complete transformation for a flow frequency of 5 Hz.

REFERENCES

[1] W.J. Buehler and R.C. Wiley, Nickel-base alloys, US Patent 3,174,851, 1965.

[2] K.Otsuka and C.M. Wayman, Shape Memory Materials, Cambridge University Press, New York, 1998.

[3] H. Funakubo, editor Shape Memory Alloys, Gordon and Breach Science Publishers, New York, 1987.

[4] D.C. Lagoudas, J.J. Mayes and M.M. Khan, Simplified SMA material model for vibration isolation, SPIE, San Diego, 2001, 69-78.

[5] C.M. Wayman, Phase transformations, non diffusive, In Physical Metallurgy, Eds. R.W. Cahn and P. Haasen, North Holland, New York, 1983

[6] R. Stalmans and J. Van Humbeeck, Shape memory alloys: functional and smart, Proceedings Smart Materials and Technologies - Sensors, Control Systems and Regulators, Prague, 1995, 135-141.

[7] O.K. Rediniotis, D.C. Lagoudas, H.Y. Jun and R.D. Allen, Fuel powered compact SMA actuator, SPIE, San Diego, 2002.

[8] L .C. Brinson, A. Bekker and S. Hwang, Temperature induced deformation in shape memory alloys, Symposium on Active Materials and Smart Structures, D. C. Lagoudas, G. L. Anderson, Eds., Society for Engineering Science 31st Annual Technical Meeting, SPIE Vol. 2427, 1994, p. 234.

[9] K.K. Ho, P. Jardine, G.P. Carman and C.J. Kim, Modeling and measuring the response times of thin film TiNi, SPIE Proceedings Smart Materials Tech., San Diego, March 1997, 118-130.

[10] D. C. Lagoudas and V.K. Kinra, Design of high frequency SMA actuators, disclosure of invention TAMUS803, Texas A&M University, College Station, TX-77840, 1993.

[11] A. Bhattacharyya, D.C.Lagoudas, A. Wang and V.K. Kinra, On the role of thermoelectric heat transfer in the design of SMA actuators: theoretical, modeling and experimental, Journal of Smart Materials and Structures, 4 (1995), 252-270.

[12] D.C. Lagoudas and Z. Ding, A modeling of thermoelectric heat transfer in shape memory alloy actuators: transient and multiple cycle solutions, Int. J. Engineering Science, 33(15) (1995), p. 2345.

[13] V. Brailkovski, F. Trochu and A. Leboeuf, Design of shape memory linear actuators, SMST-97, 1997.

[14] D. C. Lagoudas and A. Bhattacharyya, Modeling of thin layer extensional thermoelectric SMA actuators, Int. J. Solids Structures, 35(3-4) (1998), 331-362.

[15] A. Beskok and T.C. Warburton, Micro-fluidic design and fluid structure interaction analysis of a micropump, Proceedings of ASME IMECE, CA, DSC - Vol. 66, 1998, 77-84.

[16] C. Sert and A. Beskok, Time periodic forced convection cooling in micro heat spreaders, Proceedings of ASME IMECE Meeting, MEMS Vol 2, 2000, 571-580.

[17] U.H. Kurzweg, Enhanced heat conduction in fluids subjected to sinusoidal oscillations, J. Heat Transfer, 107(1985), 459-462.

[18] G. Zhang and U.H. Kurzweg, Numerical solution of time-dependent heat transfer in oscillating pipe flow, J. Thermophysics, 5(3) (1991), 401-406.

[19] E.G. Richardson, The transverse velocity gradient near the mouths of pipes in which an alternating or continuous flow air is established, Proc. Royal Soc., A42 (1929), 1-15.

[20] T. Moschandreou and M. Zamir, Heat transfer in a tube with pulsating flow and constant heat flux, Int. J. Heat and Mass Transfer, 40(10) (1995), 2461-2466.

[21] J. Sucec, Unsteady forced convective with sinusoidal duct wall generation: the conjugate heat transfer problem, Int. J. Heat and Mass Transfer, 45 (2001), 1631-1642.

[22] S.V. Patankar, Numerical Heat Transfer and Fluid Flow, Hemisphere, Washington D.C., 1980.

[23] J.G. Smits, Piezoelectric micropump with three valves working peristatically, Sensors and Actuators A, 21-23 (1990), 203-206.

[24] J. Sucec, Unsteady conjugated forced convective heat transfer in a duct with convection from the ambient, Int. J. Heat and Mass Transfer, 30(9) (1987), 1963-1970.

[25] J.G. Zhang and U.H. Kurzweg, Numerical solution of time-dependent heat transfer in oscillating pipe flow, J. Thermophysics, 5(3) (1991), 401-406.

[26] J.P Van Doormaal and G.D. Raithby, Enhancements of the SIMPLE method for predicting incompressible fluid flows, Numerical Heat Transfer, 7 (1984), 147-163.

[27] T. Zhao and P. Cheng, A numerical solution of laminar forced convection in a heated pipe subjected to a reciprocating flow, Int. J. Heat and Mass Transfer, 48 (16) (1995), 3011-3022.

[28] M. Ozawa, M. Shinoki, K. Nagoshi and E. Serizawa, Convective heat transfer in an oscillating flow, 12th Int. Heat Transfer Conference, Grenoble, France, 2002.

[29] A. Yakhot, M. Arad and G. Ben-Dor, Numerical Investigation of a laminar pulsating flow in a rectangular duct, Int. J. Numerical Methods in Fluids, 29 (1999), 935-950.

[30] J.G. Zhang, Time-dependent enhanced heat transfer in oscillating pipe flow, Ph.D. Thesis, Dept. of Aerospace Engineering, Mechanics and Engineering Science, University of Florida, Gainesville, 1988.

APPENDIX A

MODELING OF THE HEAT CAPACITY OF SMA

SMA undergoes transformation upon thermal actuation, transforming from martensite to austenite (reverse) on heating and transforming back to martensite (forward) upon cooling. Both the forward and the reverse transformations involve latent heat of phase transformation. The austenite to martensite forward transformation is an exothermic reaction and heat is released, while the reverse transformation is endothermic and requires that the latent heat of phase transformation be supplied. So it is essential to take into account this latent heat of phase transformation while modeling the heat transfer from the SMA.

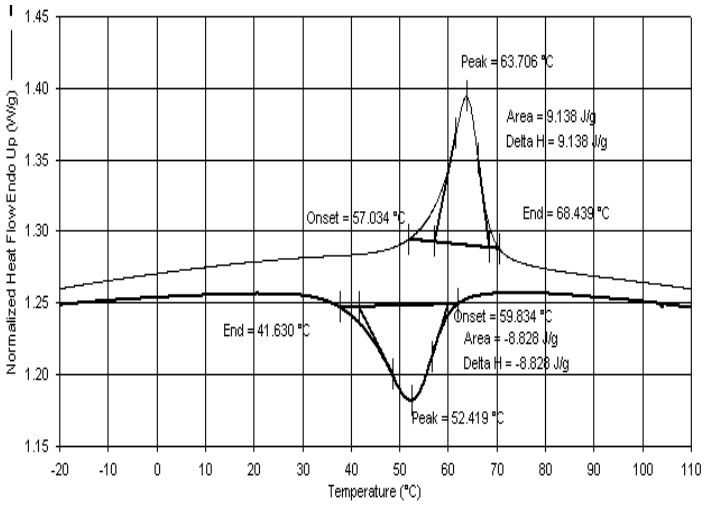

DSC test result for SMA

Consider the energy equation for one-dimensional conduction in a two-phase material with the two phases being 1 and 2. Let the material initially be in phase 1. Also let the phases be isotropic and homogeneous and have the same densities i.e $\rho_1 = \rho_2$.

$$\frac{\partial}{\partial t}(\rho_1 h_1 \xi_1 + \rho_2 h_2 \xi_2) = -\frac{\partial (q_1 \xi_1 + q_2 \xi_2)}{\partial x} \qquad \text{(A.1)}$$

Where $\rho_1, \rho_2 = \rho$ are the phase densities, h_1 and h_2 are the enthalpies of the two phases and q_1 and q_2 are the heat fluxes associated with the 2 phases. ξ is the volume fraction and by definition we have $\xi_1 + \xi_2 = 1$.

By Fourier's law, $q = -k\frac{\partial T}{\partial x}$, where k is the thermal conductivity and T is the temperature. So we have,

$$\left[\frac{\partial(\rho h_2)}{\partial T} + \{\frac{\partial(\rho h_1)}{\partial T} - \frac{\partial(\rho h_2)}{\partial T}\}\xi_1 + (\rho h_1 - \rho h_2)\frac{\partial \xi_1}{\partial T}\right]\frac{\partial T}{\partial t} = \left[k_2 + (k_1 - k_2)\xi_1\right]\frac{\partial^2 T}{\partial x^2} \quad \text{(A.2)}$$

With $k_1 = k_2 = k$, we get

$$\rho C_{pw}\frac{\partial T}{\partial t} = k\frac{\partial^2 T}{\partial x^2} \quad \text{(A.3)}$$

where

$$\rho C_{pw} = \frac{\partial(\rho h_2)}{\partial T} + \{\frac{\partial(\rho h_1)}{\partial T} - \frac{\partial(\rho h_2)}{\partial T}\}\xi_1 + (\rho h_1 - \rho h_2)\frac{\partial \xi_1}{\partial T} \quad \text{(A.4)}$$

$$C_1 = \frac{\partial h_2}{\partial T}, C_2 = \frac{\partial h_2}{\partial T}$$

and C_1 and C_2 are the specific heat for phases 1 and 2 respectively.

Consider the transformation of phase 1 into phase 2. Let the transformation begin at a temperature T_s

$$h_1 = H + \int_{T_s}^{T} C_1 dT$$

$$h_2 = \int_{T_s}^{T} C_2 dT$$

If we assume ρ, C_1 and C_2 to be constants, then we have the apparent (effective) heat capacity at any point during the transformation as

$$C_{pw}(T) = C_1 + (C_2 - C_1)\xi_1 + H\frac{\partial \xi_1}{\partial T} \quad \text{(A.5)}$$

Further assuming $C_1 = C_2 = C_p^0$, we get

$$C_{pw}(T) = C_p^0 + H\frac{\partial \xi_1}{\partial T} \tag{A.6}$$

The second term on the right hand side represents the contribution due to the phase transformation and it is non-zero only when the temperature is between the start and end of transformation temperatures. Outside that range, the specific heat is equal to a constant value of C_p^0.

Based on DSC tests, Bhattacharyya et al. proposed the following empirical relationship for the specific heat of a SMA to account for the latent heat of transformation.

For forward transformation (cooling),

$$C_{pw}^f = C_{pw}^0 + H\frac{\ln(100)}{|M^{st} - M^{ft}|}\exp\left[-\frac{2\ln(100)}{|M^{st} - M^{ft}|}\left|T - \frac{M^{st} + M^{ft}}{2}\right|\right], \quad M^{fi} \le T \le M^{st} \tag{A.7}$$

And

For reverse transformation (heating),

$$C_{pw}^r = C_{pw}^0 + H\frac{\ln(100)}{|A^{st} - A^{fi}|}\exp\left[-\frac{2\ln(100)}{|A^{st} - A^{fi}|}\left|T - \frac{A^{st} + A^{fi}}{2}\right|\right], \quad A^{st} \le T \le A^{fi} \tag{A.8}$$

Where C_p^0 is the constant specific heat of the martensitic and austenitic phases, H is the latent heat of phase transformation and M^s, A^s, M^f and A^f are the martensite and austenite start and martensite and austenite finish temperatures, respectively. These are determined from the plots from the DSC test. The latent heat H is equal to the area under the specific heat curve.

APPENDIX B

NON-DIMENSIONAL ENERGY EQUATIONS

Non-dimensional energy equations for unidirectional flow

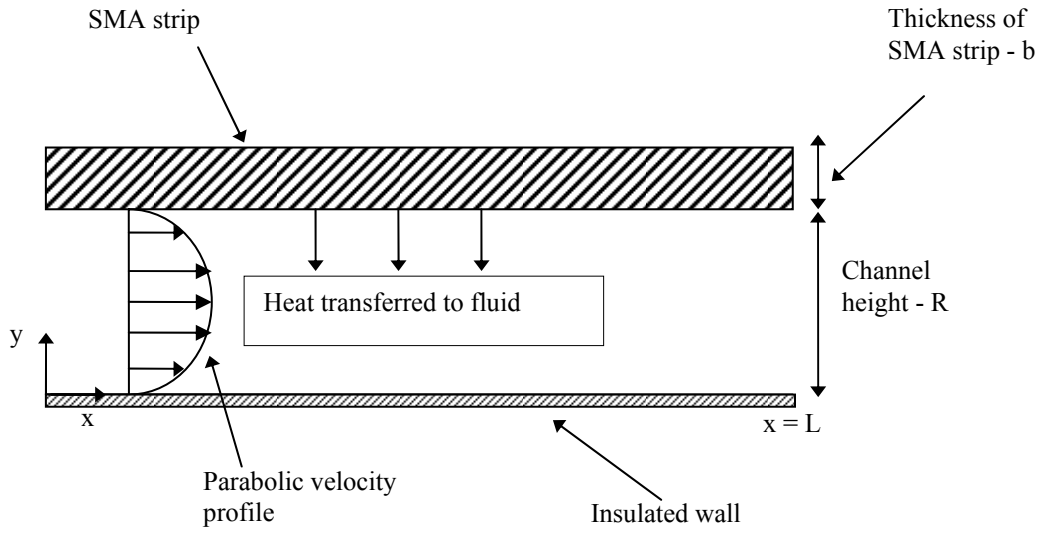

The energy equation for the fluid is given by

$$\rho_f C_{pf} \frac{\partial T_f}{\partial t} + \rho_f C_{pf} \left(u \frac{\partial T_f}{\partial x} + v \frac{\partial T_f}{\partial y} \right) = k_f \left(\frac{\partial^2 T_f}{\partial x^2} + \frac{\partial^2 T_f}{\partial y^2} \right) \tag{B.1}$$

In a unidirectional flow v = 0. Also axial conduction is much smaller than convection and so we can negect the first term inside the bracket on the right hand side. So we get

$$\rho_f C_{pf} \frac{\partial T_f}{\partial t} + \rho_f C_{pf} u(y) \frac{\partial T_f}{\partial x} = k_f \left(\frac{\partial^2 T_f}{\partial x^2} + \frac{\partial^2 T_f}{\partial y^2} \right) \tag{B.2}$$

Let $\theta_f = \dfrac{k_f (T - T_E)}{qbR}, \tau = \alpha_f t / R^2, Y = y / R, X = \alpha_f x / (R^2 U_{\max}), B = \dfrac{\rho_w C_{Pw} b}{\rho_f C_{Pf} R}$

Using the definitions above, we can non-dimensionalise the simplified energy equation to give

$$\frac{\partial \theta_f}{\partial \tau} + 4(Y - Y^2)\frac{\partial \theta_f}{\partial X} = \frac{\partial^2 \theta_f}{\partial Y^2} \tag{B.3}$$

The second term on the LHS represents convection in a flow with a parabolic velocity profile.

The energy balance for the SMA strip is

$$\rho_w C_{pw} b \frac{\partial T_w}{\partial t} = k_w \left(\frac{\partial^2 T_w}{\partial x^2} + \frac{\partial^2 T_w}{\partial y^2} \right) + f q_g b - k_w \frac{\partial T_w}{\partial y} \tag{B.4}$$

The first two bracketed terms on the right hand side represent axial and transverse conduction within the SMA. The third term represents the heat supplied to the SMA. The last term on the RHS represents the heat lost by the SMA to the fluid due to the temperature gradient.

AT the interface of the SMA strip (wall) and the fluid, there is a continuity of temperature and heat flux. In other words, the temperature of the SMA strip is equal to the fluid temperature at the interface of the SMA strip and the fluid. Also the heat lost by the SMA strip is equal in magnitude to the heat gained by the fluid. This is written mathematically as

$$\begin{aligned} T_w \,|_{y=R} &= T_f \,|_{y=R} \\ k_w \left.\frac{\partial T_w}{\partial x}\right|_{y=R} &= -k_f \left.\frac{\partial T_f}{\partial x}\right|_{y=R} \end{aligned} \tag{B.5}$$

Substituting these two equations in the energy balance for the SMA strip, we get

$$\rho_w C_{pw} b \frac{\partial T_f}{\partial t} = k_w \left(\frac{\partial^2 T_f}{\partial x^2} + \frac{\partial^2 T_f}{\partial y^2} \right) + f q_g b + k_f \frac{\partial T_f}{\partial y} \tag{B.6}$$

Using the previously defined non-dimensional variables, this equation becomes

$$B\frac{\partial\theta_w}{\partial\tau}-(\frac{\partial\theta_w}{\partial Y})=f \tag{B.7}$$

Non-dimensional energy equations for oscillating flow

The energy equation for the fluid is

$$\rho_f C_{pf}\frac{\partial T_f}{\partial t}+\rho_f C_{pf}\left(u\frac{\partial T_f}{\partial x}+v\frac{\partial T_f}{\partial y}\right)=k_f\left(\frac{\partial^2 T_f}{\partial x^2}+\frac{\partial^2 T_f}{\partial y^2}\right) \tag{B.8}$$

Let

$$X=x/R, Y=y/R, U=u/u_{\max}, V=v/u_{\max}, \tau=\omega t, \theta=\frac{T-T_E}{T_r-T_E}, B=\frac{\rho_w C_{Pw} b}{\rho_f C_{Pf} R}*\mathrm{Re}_w\,\mathrm{Pr}$$

With these these non-dimensional variables, the energy equation for the fluid becomes

$$\frac{\partial\theta_f}{\partial\tau}+\frac{A_0}{\pi}\left[U\frac{\partial\theta_f}{\partial X}+V\frac{\partial\theta_f}{\partial Y}\right]=\frac{1}{\mathrm{Re}_w\,\mathrm{Pr}}\left[\frac{\partial^2\theta_f}{\partial X^2}+\frac{\partial^2\theta_f}{\partial Y^2}\right] \tag{B.9}$$

The y-component of velocity is not zero in an oscillating flow but it is small compared top the x-component. So the second term inside the bracket on the left hand side is small and so it is neglected.

The energy balance for the SMA strip is given by

$$\rho_w C_{pw} b\frac{\partial T_w}{\partial t}=k_w\left(\frac{\partial^2 T_w}{\partial x^2}+\frac{\partial^2 T_w}{\partial y^2}\right)+fq_g b-k_w\frac{\partial T_w}{\partial y} \tag{B.10}$$

The transverse conduction within the SMA strip (second term inside the bracket on the RHS) is neglected because the biot number is very small.

Using the non-dimensional variables defined above, this equation changes to

$$B\frac{\partial\theta_w}{\partial\tau}-(\frac{\partial\theta_w}{\partial Y})=f+\left(\frac{k_w}{k_f}\right)\left(\frac{b}{R}\right)\frac{\partial^2\theta_w}{\partial X^2} \tag{B.11}$$

VITA

Rajagopal Pachalla Seshadri was born in India. He obtained his Bachelor of Technology in naval architecture from the Indian Institute of Technology, Madras, India, in July 2000. Upon completion of his master's work, he plans to pursue a Ph.D. degree.

His permanent address is:
No. 28, Vedachalam Garden,
Mandeiveli,
Madras 600028,
Tamil Nadu, India
Phone: (91)44- 24937044
email: rajagopal@tamu.edu
raja400@hotmail.com